Ionosphere Scintillations at low and high latitudes Observations and Modelling

ESA Monitor network of receivers

Y. Béniguel
IEEA, France
beniguel@ieea.fr

Contents

- **Low Latitudes**
  - **Occurrence and probabilities**
  - **Raw data analysis**
- **High Latitudes**
  - **Scintillation occurrence dependencies**
- **Modelling**
  - **GISM**
- **Extreme Events**
  - **EGNOS**

Ionosphere Variability

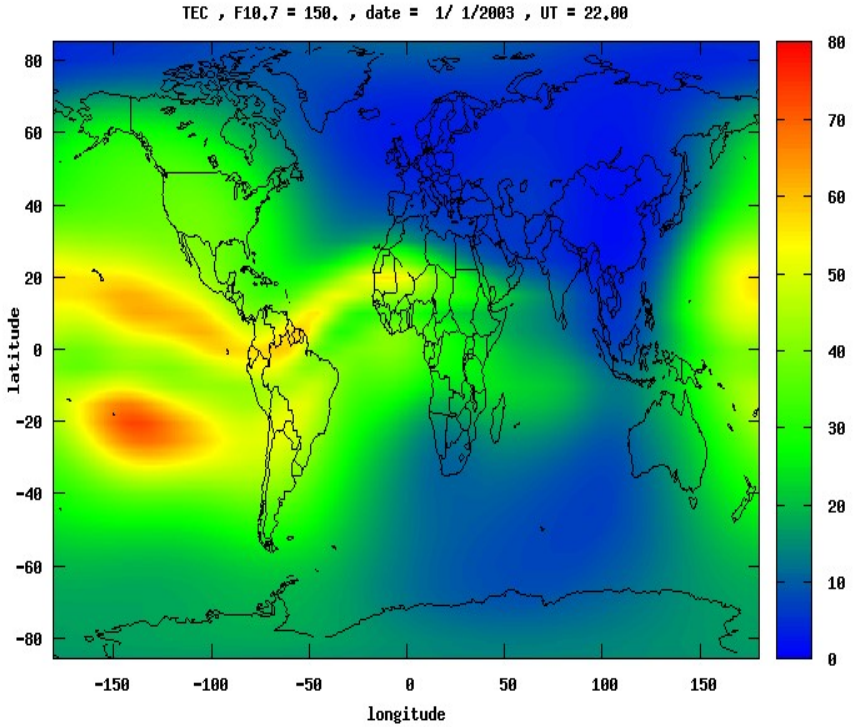

TEC Map

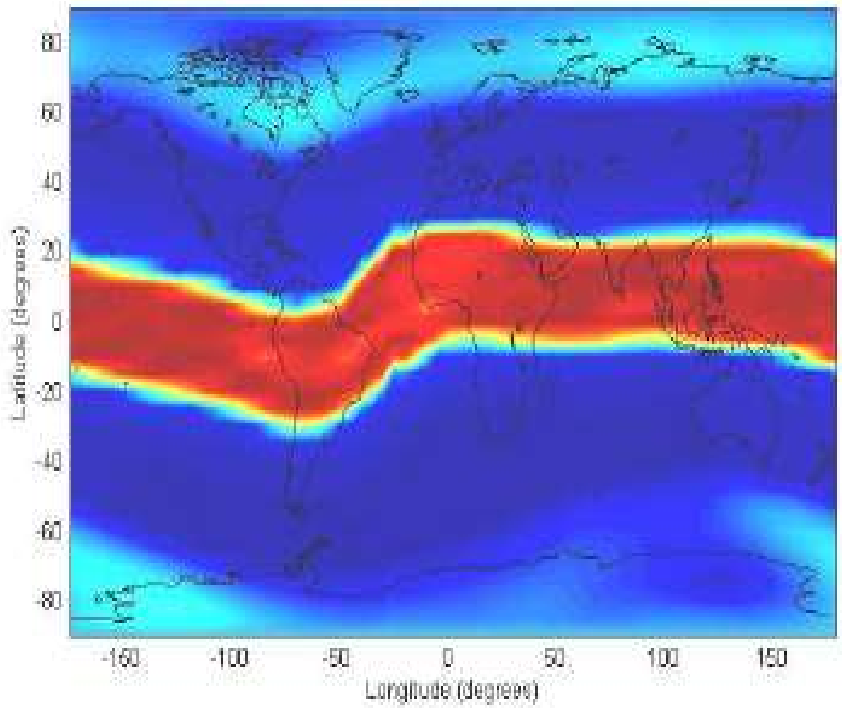

Location of turbulences

(cumulative map)

Section 1

Turbulent Ionosphere
The Low Latitudes

Medium Radar Observations

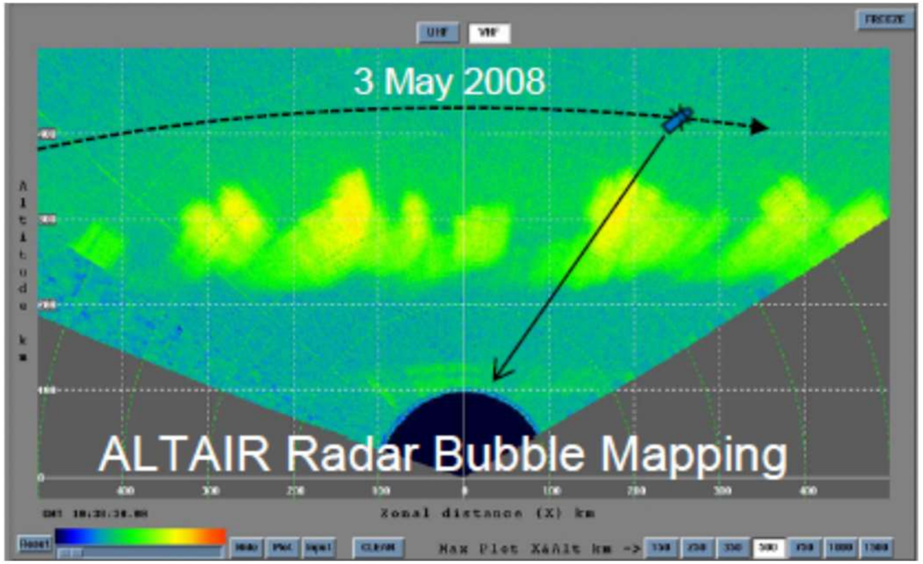

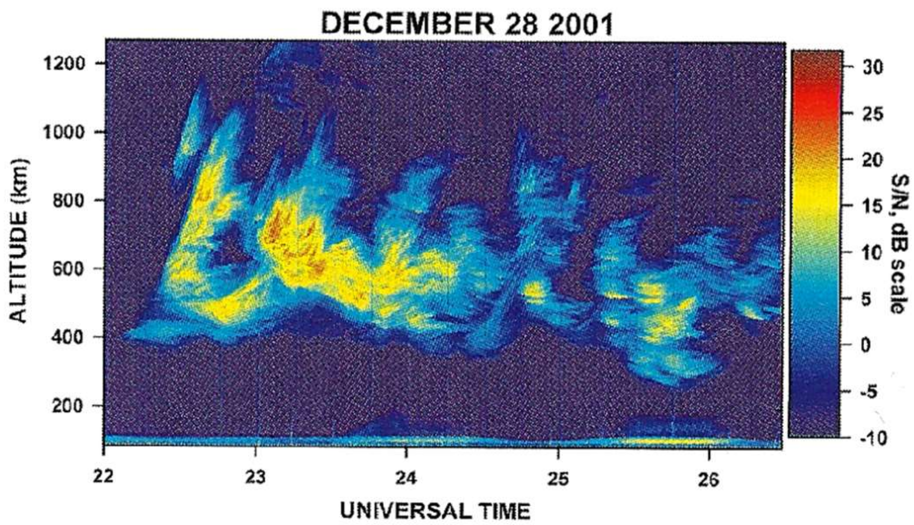

Observations at Kwajalen Islands
Courtesy K. Groves, BC

Observations in Brazil
Courtesy E. de Paula, INPE

The vertical extent may reach hundreds of kilometers

Physical Mechanism

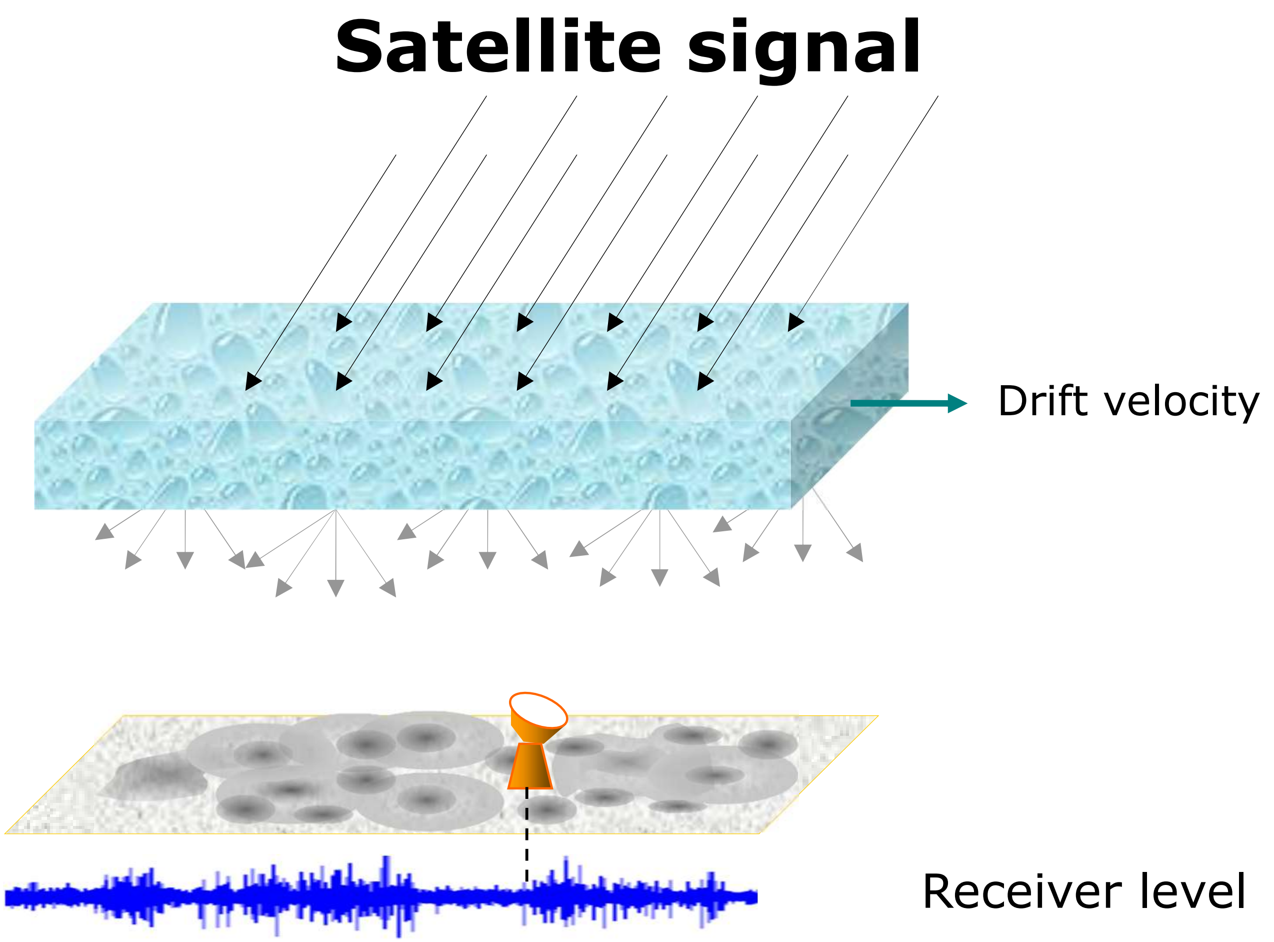

The scattering pattern changes rapidly in time and space creating fast fluctuations (scintillations) at receiver level

Scintillation on Galileo Satellites L1 vs E5a

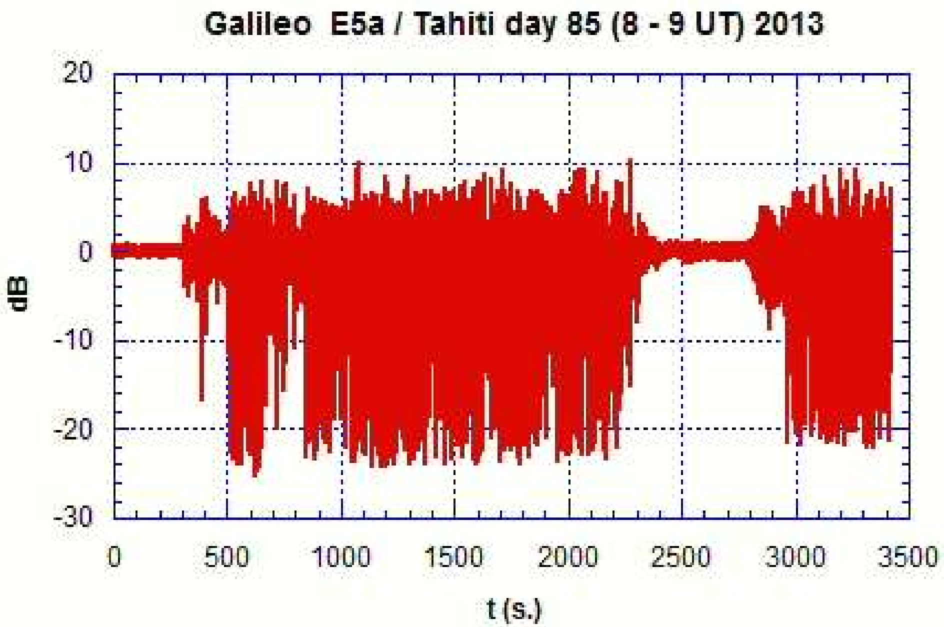

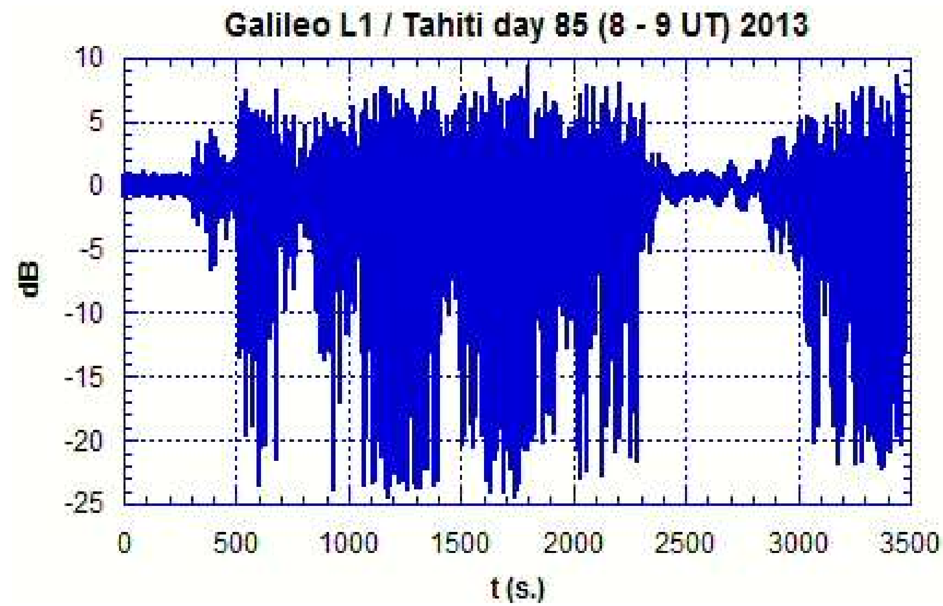

Characterisation of Signal Fluctuations Indices Definition

$$S_4^2 = \frac{\langle I^2 \rangle - \langle I \rangle^2}{\langle I \rangle^2} \qquad \text{with} \qquad I = |E|^2$$

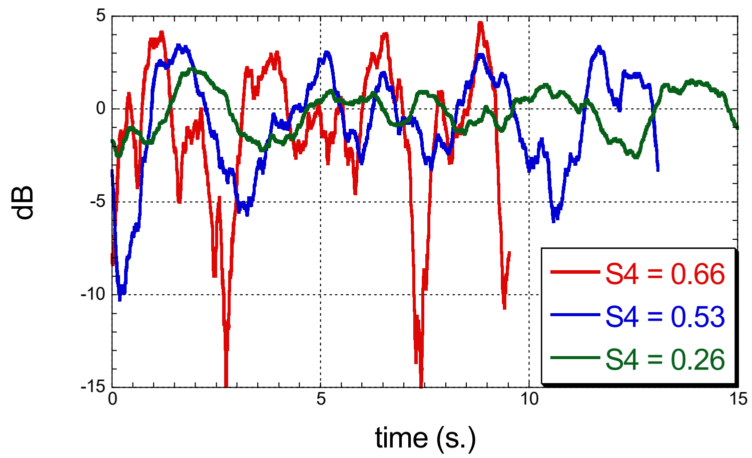

$$\sigma_\Phi^2 = \langle \Phi^2 \rangle - \langle \Phi \rangle^2$$

0 < S4 < 1

$$ROTI = \langle \left(\frac{\partial\, TEC}{\partial\, t} \right)^2 \rangle - \langle \frac{\partial\, TEC}{\partial\, t} \rangle^2$$

- **Decorrelation time**

Example: one Day of Scintillation Occurrence Dependency on Local Time and on the Elevation Angle

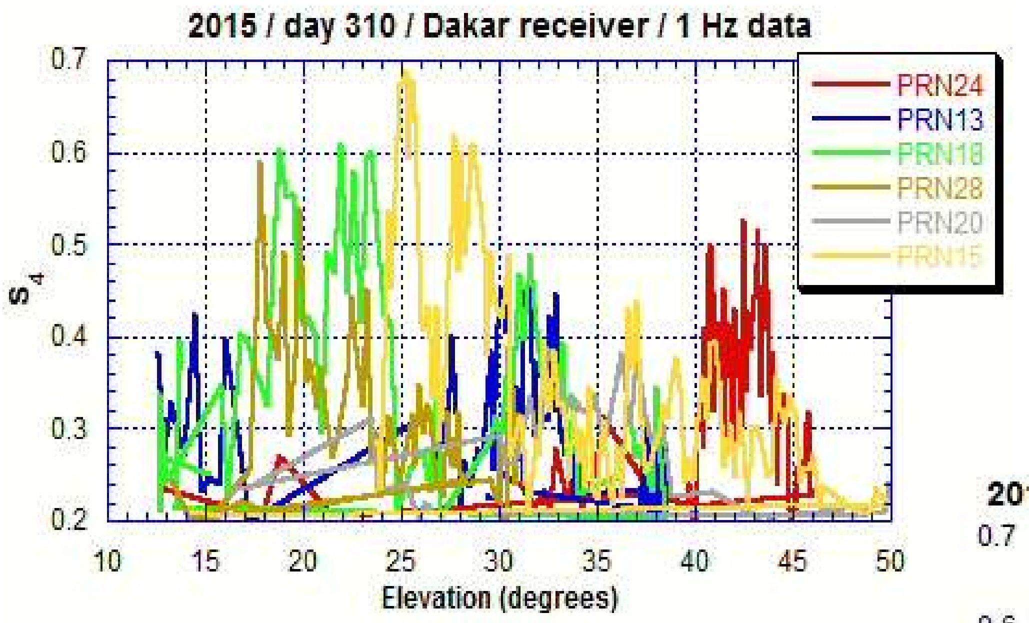

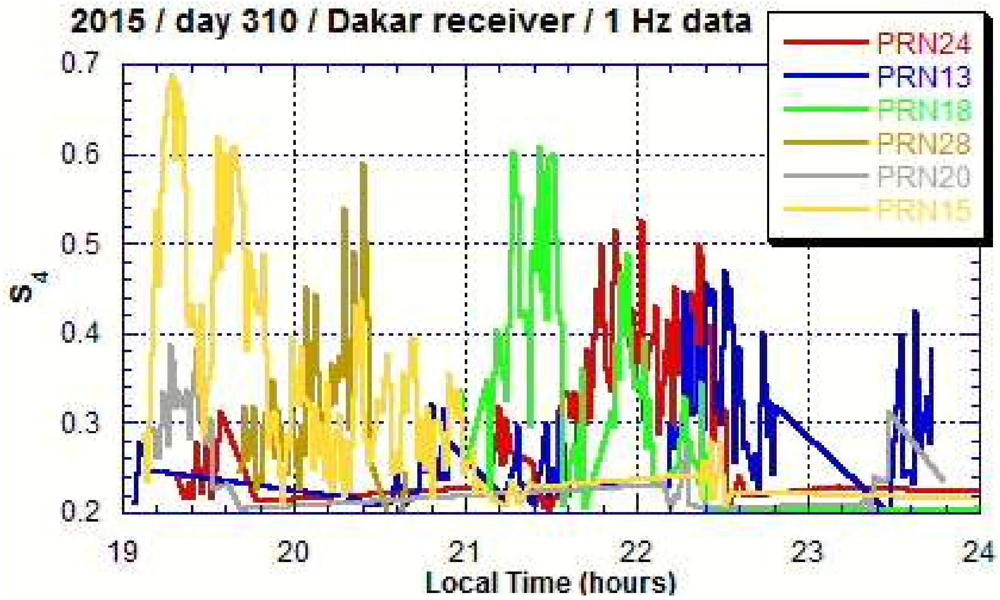

ESA Measurement Campaigns

- Prediction of Ionospheric scintillations (PRIS) (2006 – 2008) *
- MONitoring of Ionosphere by innovative Techniques coordinated Observations and Resources (MONITOR) (2010– 2014) *
- MONITOR 2 (2014 – 2018) *
- e-MONITOR (2020 –) **

F10.7cm Radio Flux Progression

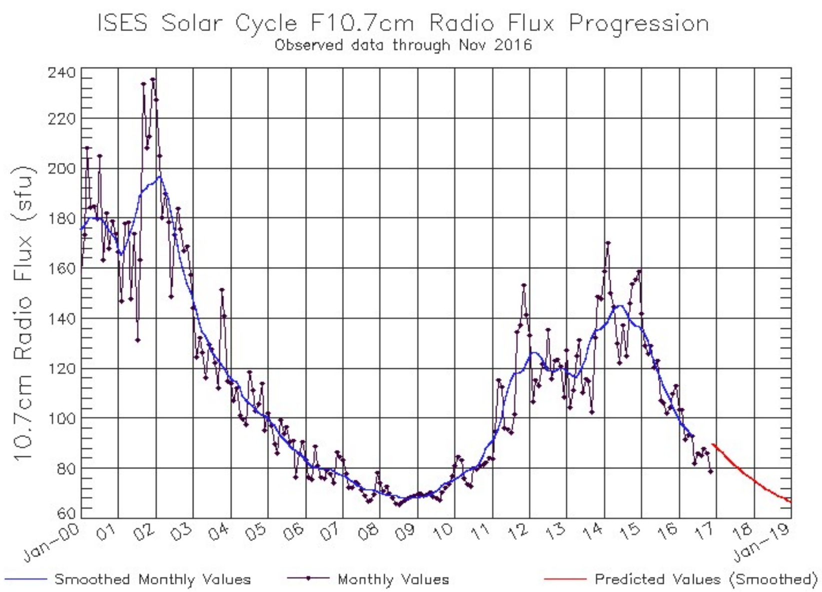

* IEEA + DLR, UPC, QINETIQ, ICTP, TAS, FMI, UWM, …

** DLR + IEEA, UPC, ICTP, NLR, Airbus DE

MONITOR Scintillations Receivers Network

MONITOR Content

- Introduction
- Project partners
- Documentation
- Stations map - data
- Stations map - products
- Search input data
- Search products
- Data policy
- Contact

STATIONS MAP - DATA TYPES

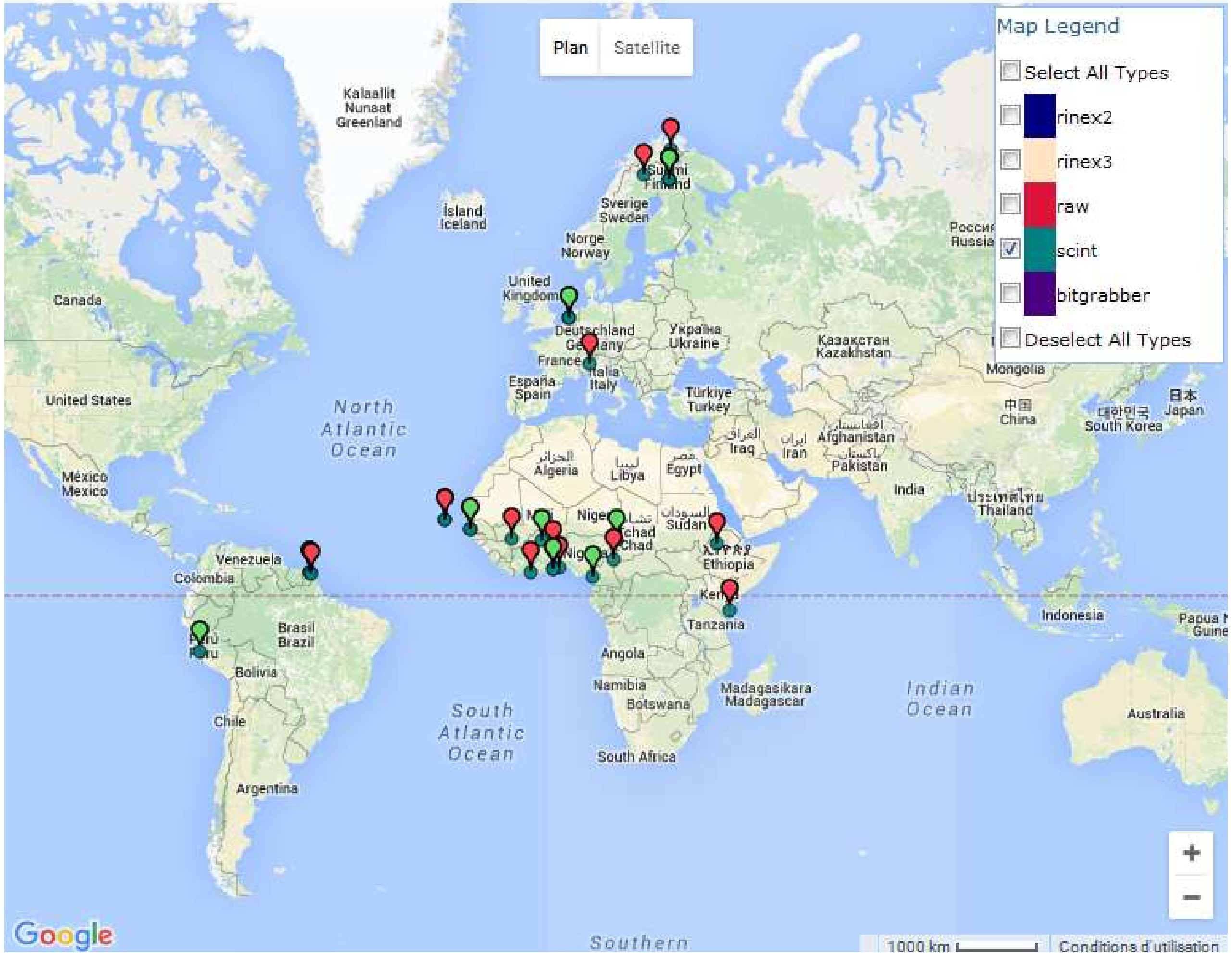

Station Name	Project Operating Period	Latitude	Longitude	Equipment	Sampling frequency
Tahiti (French Polynesia)	Monitor 1 09/2012 – 09/2014	17.55° S	210.39° E	PolaRxS	50 Hz
Lima (Peru)	Monitor 1 09/2011 – 11/2016	12.18° S	282.58° E	GSV4004B	50 Hz
Cayenne (French Guyana)	Monitor 1 05/2006 – 04/2016	4.8° N	307.63° E	GSV4004B	50 Hz
Cape Verde	Monitor 1 12/2012 – 09/2015	16.73° N	337.07° E	GSV4004B + GISMO	50 Hz
Malindi (Kenya)	Monitor 1 04/2013 – 12/2013	3. ° S	40.72° E	PolaRxS	50 Hz
Sodankylä (Finland)	Monitor 1 11/2011 -	67.25° N	26.36° E	GSV4004B	50 Hz
Kevo (Finland)	Monitor 1 03/2013 -	69.75°N	27.019° E	GSV4004B	50 Hz
Dakar (Senegal)	SAGAIE	14.765° N	342.62° E	PolaRxS + Novatel FlexPack 6	50 Hz / 1 Hz
Ouagadougou (Burkina Fasso)	SAGAIE	12.368° N	358.47° E	Novatel FlexPack 6	1 Hz
Lomé (Togo)	SAGAIE	6.132° N	1.223° E	PolaRxS + Novatel FlexPack 6	50 Hz / 1 Hz
Douala (Cameroon)	SAGAIE	4.049° N	9.699° E	Novatel FlexPack 6	1 Hz
N'Djamena (Chad)	SAGAIE	12.113° N	15.048° E	Novatel FlexPack 6	1 Hz
Abidjan (Ivory Coast)	Monitor 2 05/2015 -	5.27° N	356.08 E	PolaRxS	50 Hz
Cotonou (Benin)	Monitor 2 07/2015 -	6.352° N	2°383 E	PolaRxS	50 Hz
Niamtogou (Togo)	Monitor 2 07/2015 -	9.774° N	1.098° E	PolaRxS	50 Hz
Bamako (Mali)	Monitor 2 07/2015 -	12.540° N	7.949 W	PolaRxS	50 Hz
Bahir Dar (Ethiopia)	Monitor 2 07/2014 -	11.598° N	37°396° E	GSV4004B	50 Hz
Kiruna (Sweden)	Monitor 2 04/2015 -	67.743° N	21.06° E	PolaRxS	50 Hz

Low Latitudes Receivers Network

Station Name	Project	Latitude	Longitude	Equipment	Sampling frequency
Dakar (Senegal)	SAGAIE	14.765° N	342.62° E	PolaRxS + Novatel FlexPack 6	50 Hz / 1 Hz
HOuagadougou (Burkina Fasso)	SAGAIE	12.368° N	358.47° E	Novatel FlexPack 6	1 Hz
Lomé (Togo)	SAGAIE	6.132° N	1.223° E	PolaRxS + Novatel FlexPack 6	50 Hz / 1 Hz
Douala (Cameroon)	SAGAIE	4.049° N	9.699° E	Novatel FlexPack 6	1 Hz
N'Djamena (Chad)	SAGAIE	12.113° N	15.048° E	Novatel FlexPack 6	1 Hz
Abidjan (Ivory Coast)	Monitor 2	5.27° N	356.08 E	PolaRxS	50 Hz
Cotonou (Benin)	Monitor 2	6.352° N	2°383 E	PolaRxS	50 Hz
Niamtogou (Togo)	Monitor 2	9.774° N	1.098° E	PolaRxS	50 Hz
Bamako (Mali)	Monitor 2	12.540° N	7.949 W	PolaRxS	50 Hz

Number of Events (> 1 mn)
Northern Hemisphere vs Southern Hemisphere

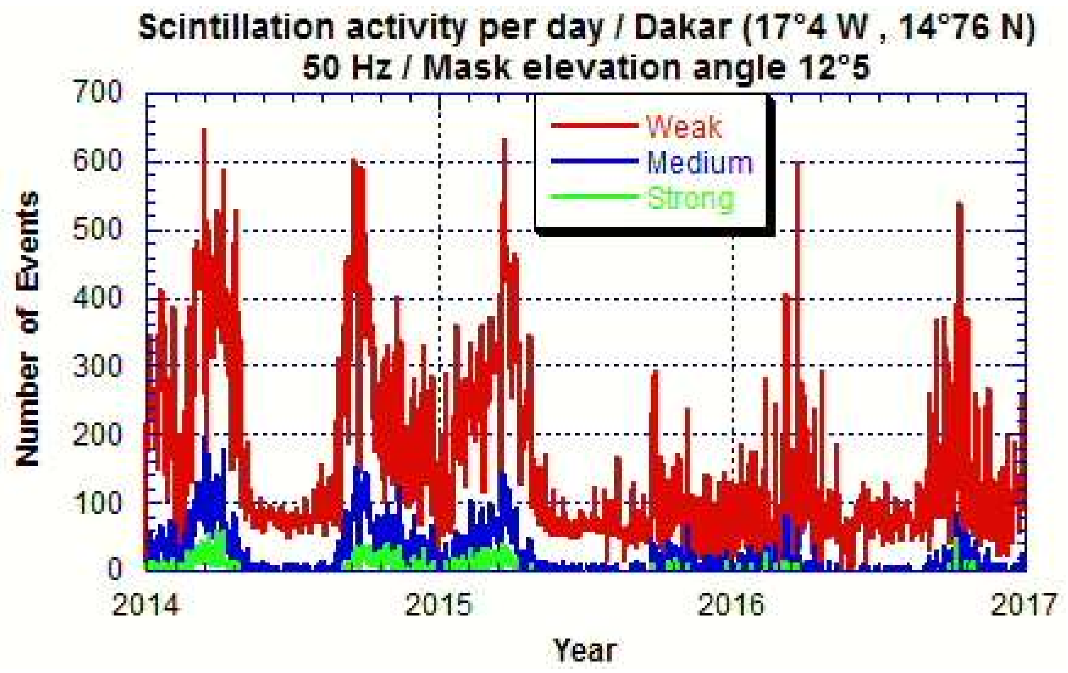

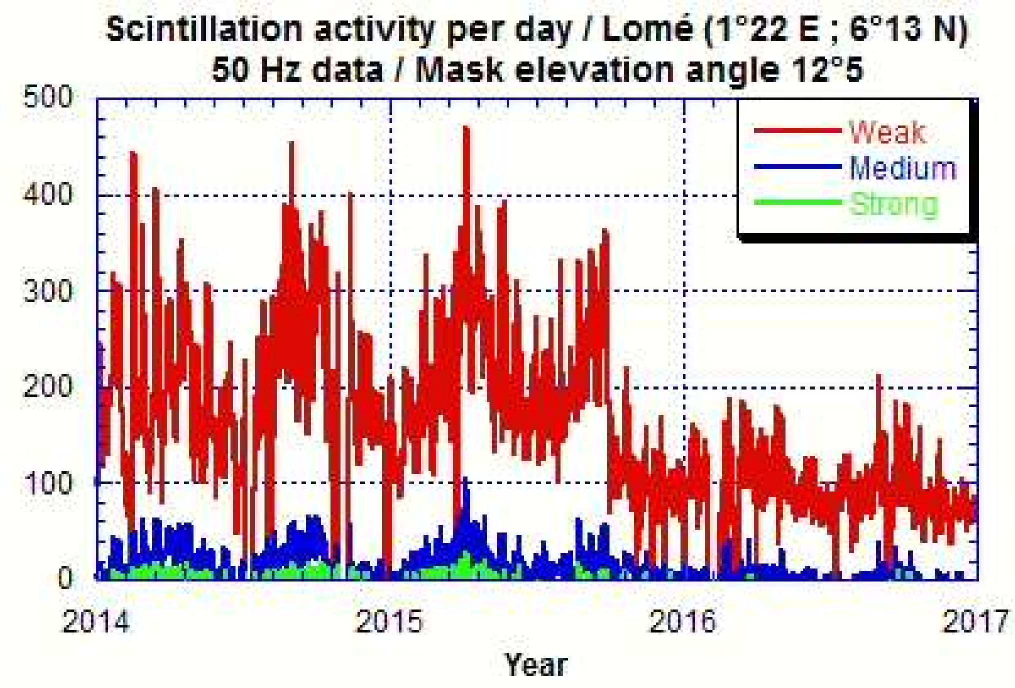

North hemisphere wrt magnetic equator

South hemisphere wrt magnetic equator

weak : 0.2 < S4 < 0.4 medium : 0.4 < S4 < 0.6 strong : S4 > 0.6

Number of Events (1 mn)
1 Hz vs 50 Hz

North hemisphere wrt magnetic equator

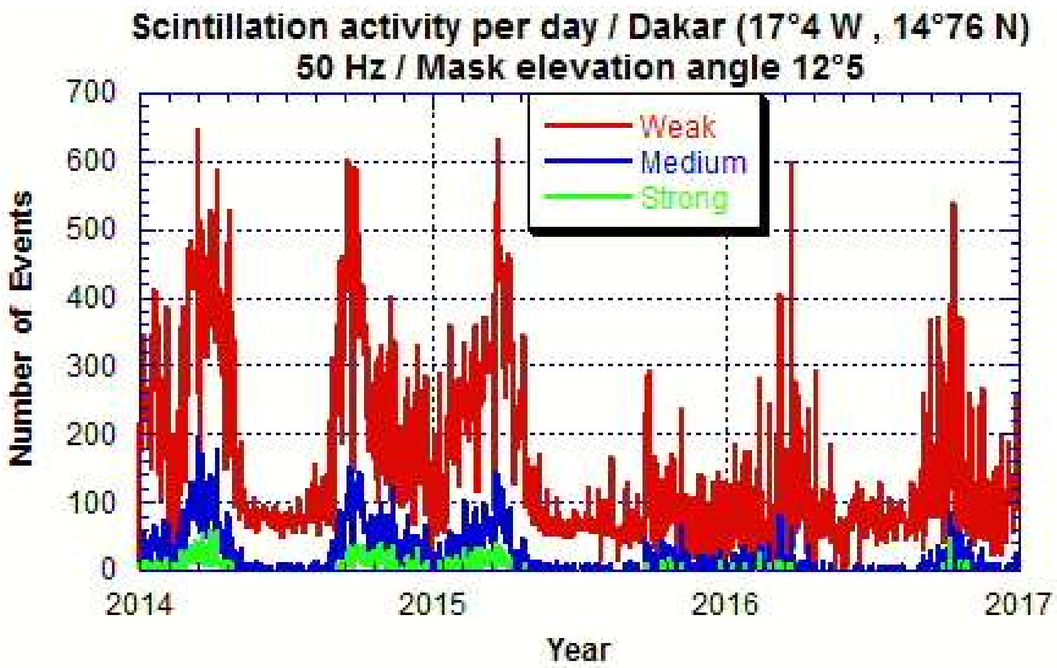

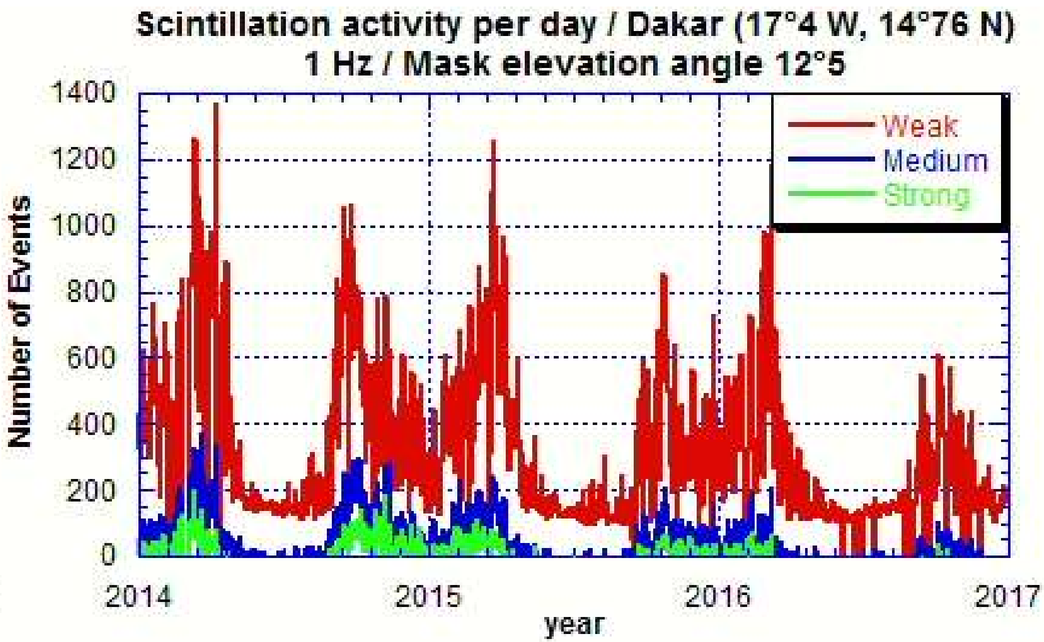

50 Hz data

1 Hz data

About 2 times more events

Probability of scintillation occurrence
1 Hz vs 50 Hz recording / Comparison of results

1 Hz

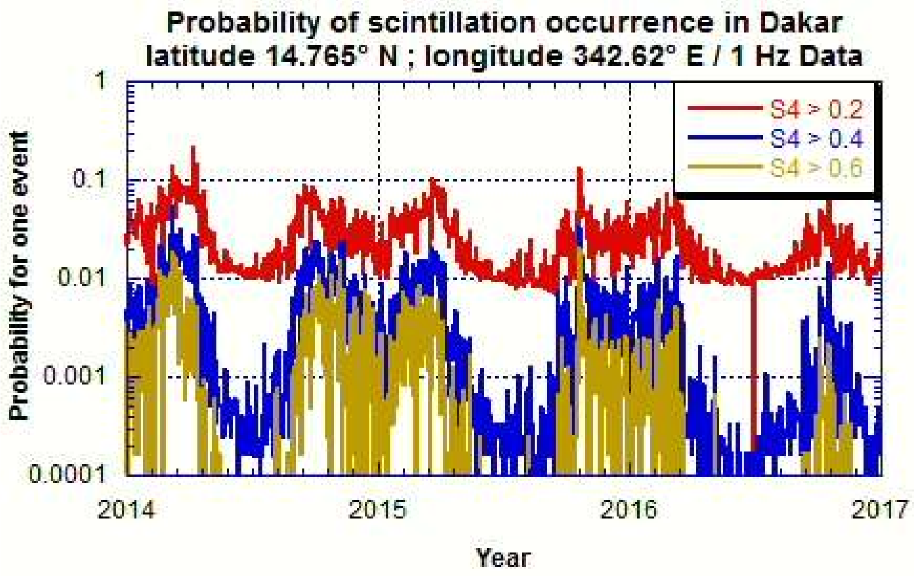

50 Hz

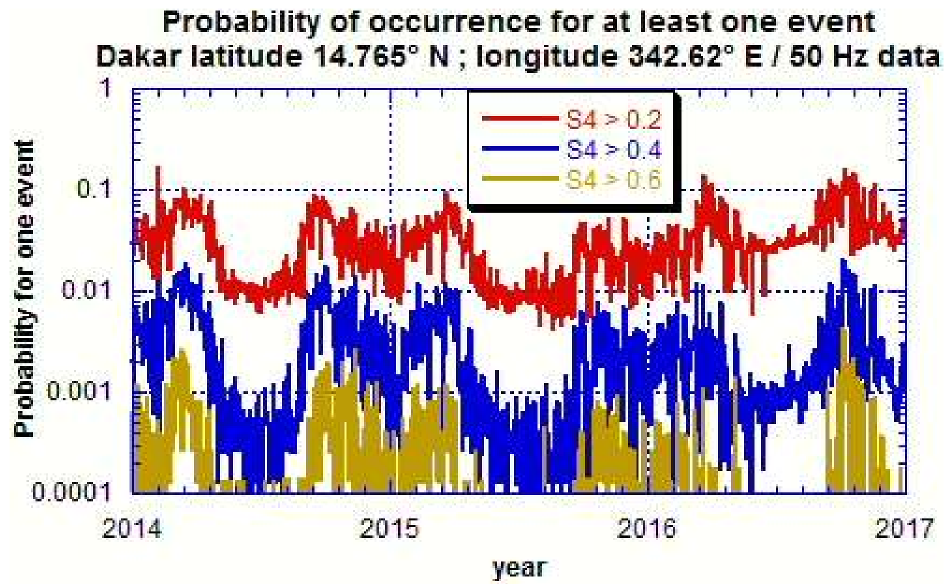

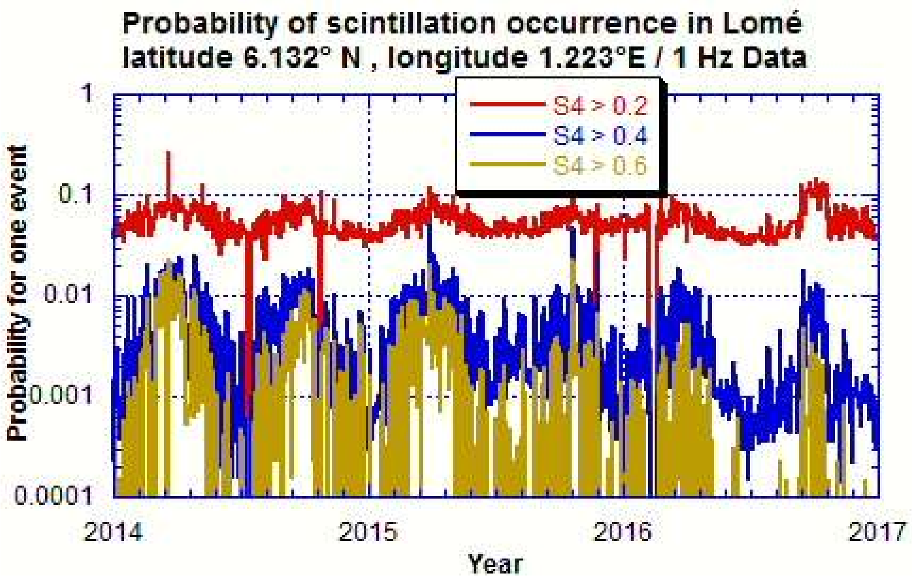

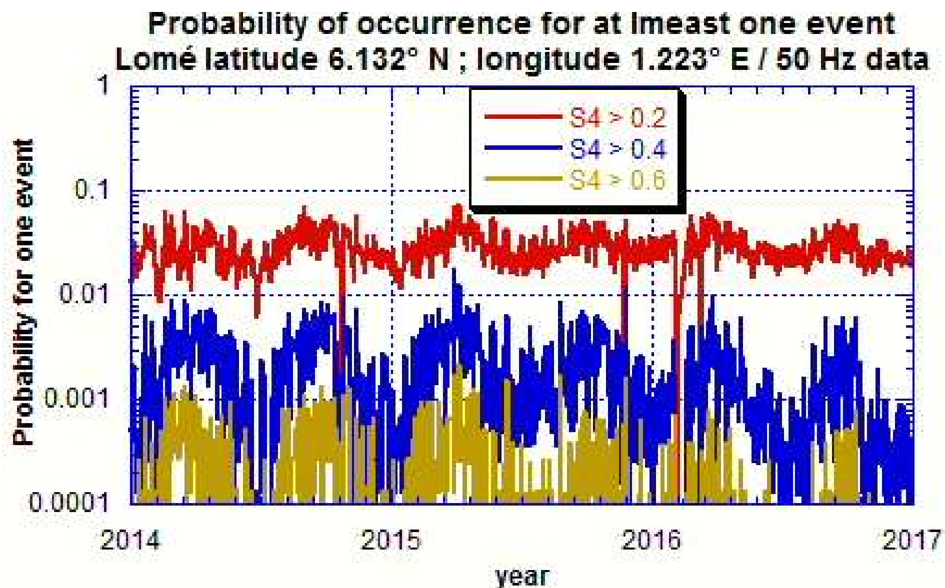

How many links simultaneously affected with scintillations

North hemisphere

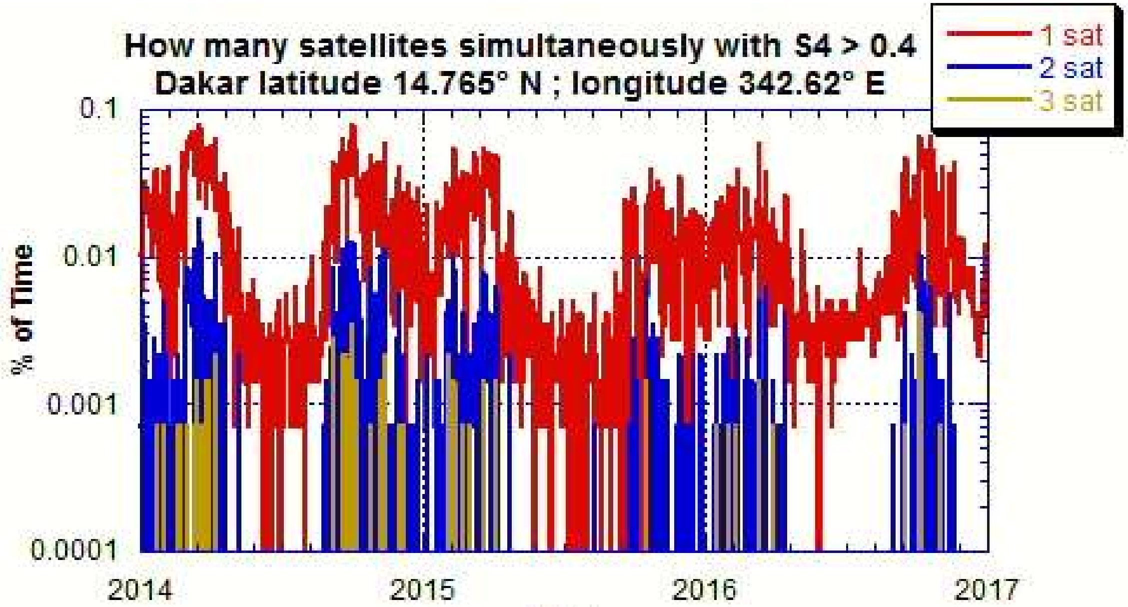

50 Hz data

South hemisphere

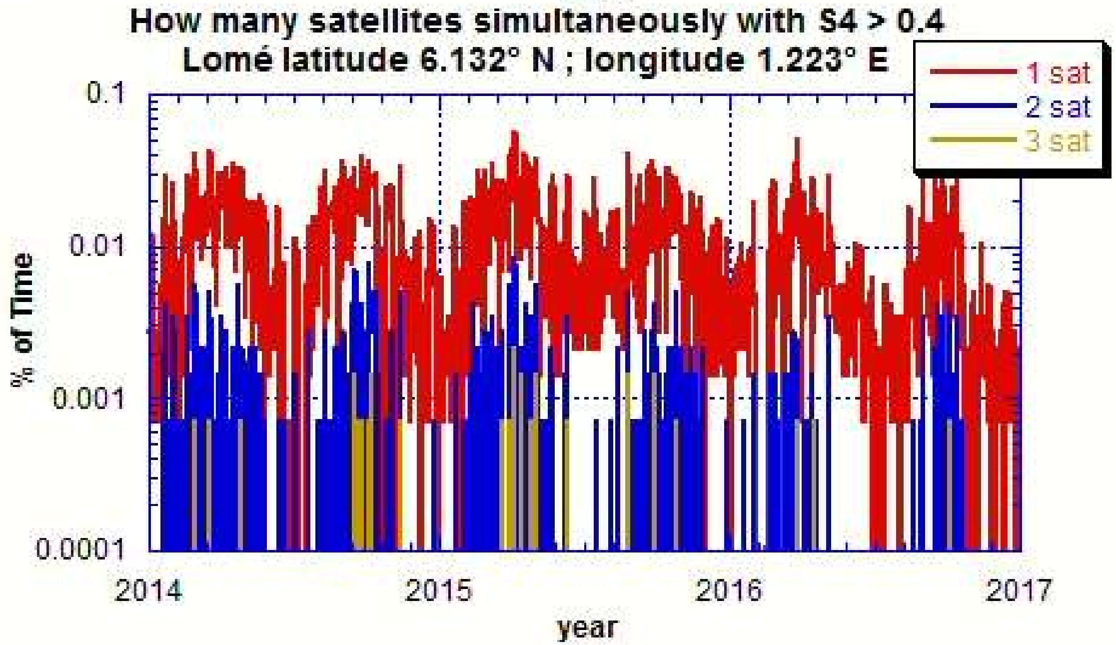

Dependency on the Latitude

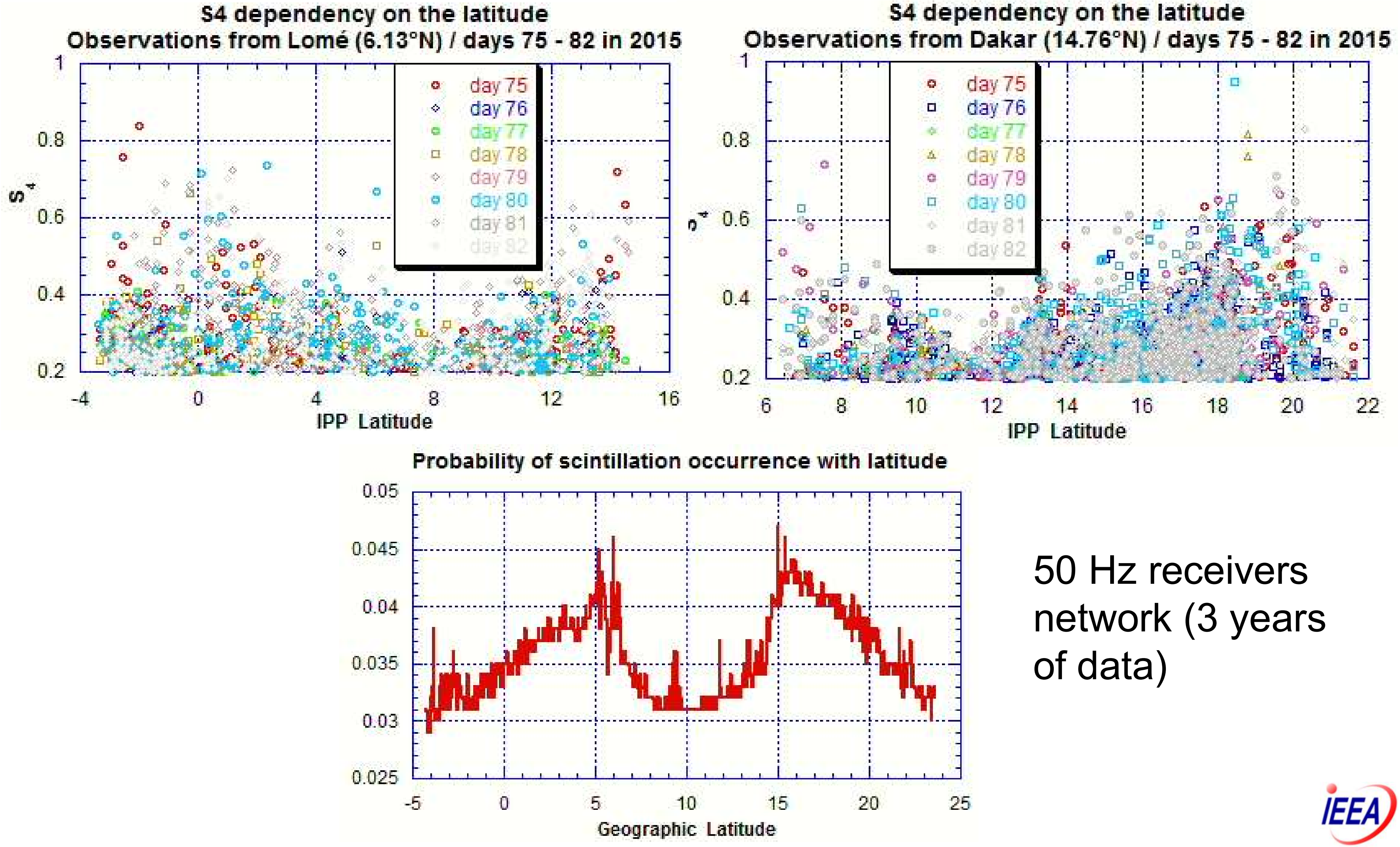

50 Hz receivers network (3 years of data)

Dependency on Local Time

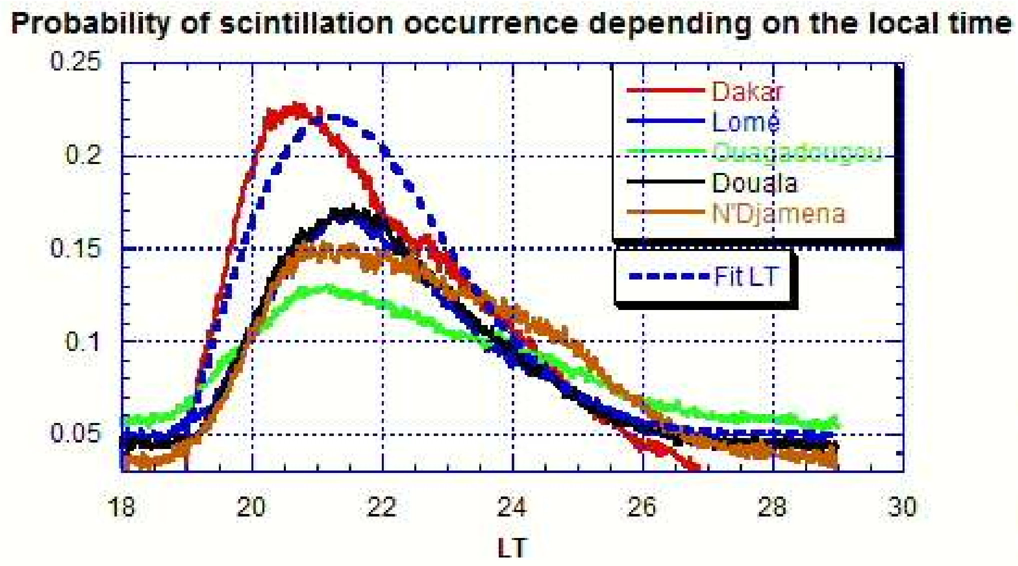

$$f(t) = 0.05 + 0.63\ \frac{t - 19}{\sigma^2}\ \exp\left(-\ (t - 19)^2 / (2\sigma^2)\right)$$

with $\sigma^2 = 5$ and t in hours

$$\int_{19\ \text{pm}}^{2\ \text{am}} f(t)\ dt = 0.98$$

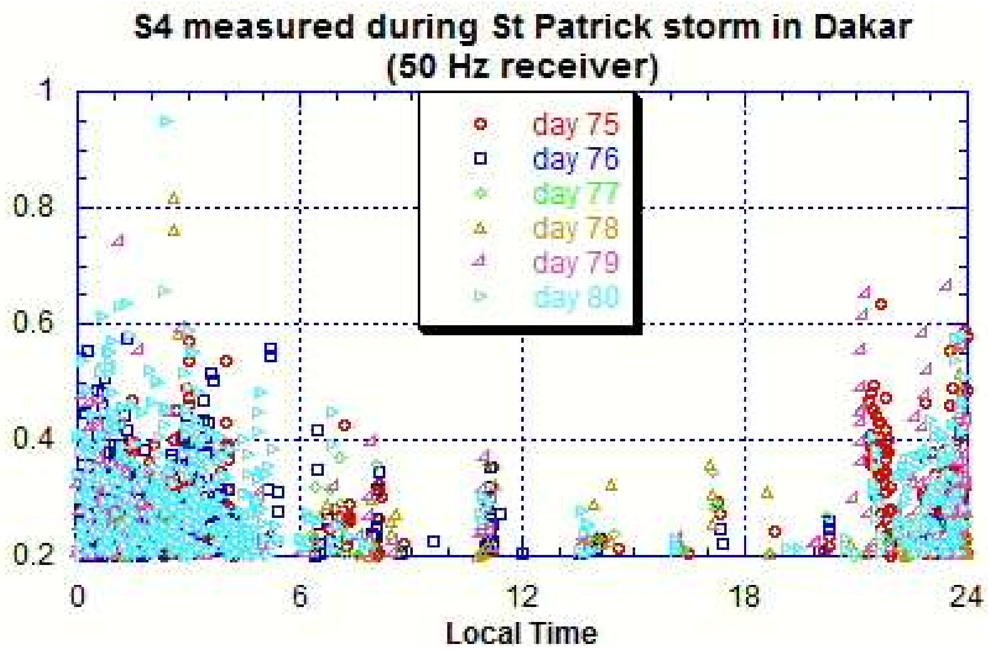

Scintillation also at day time

Raw Data Analysis

Raw Data Analysis

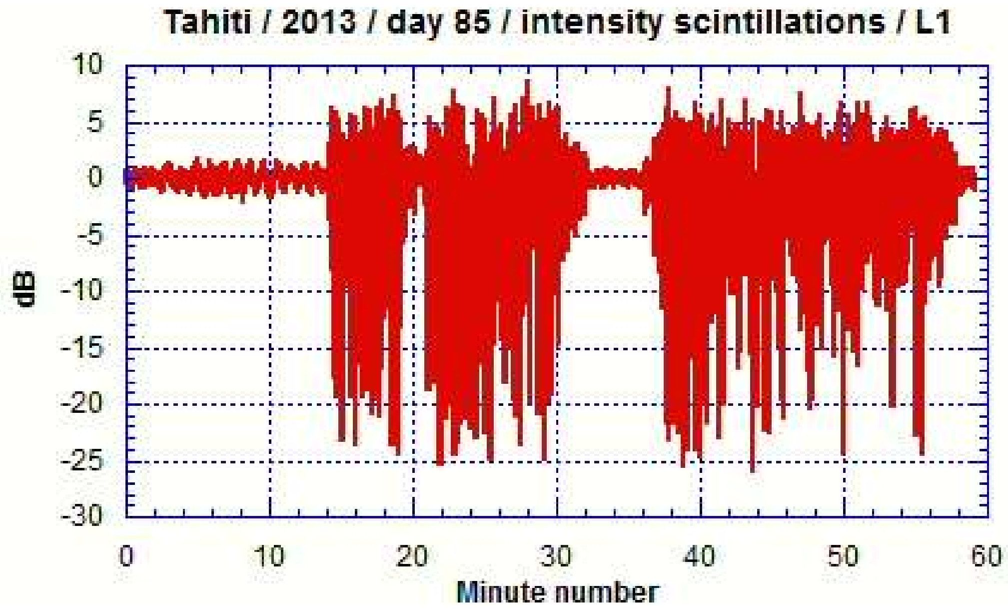

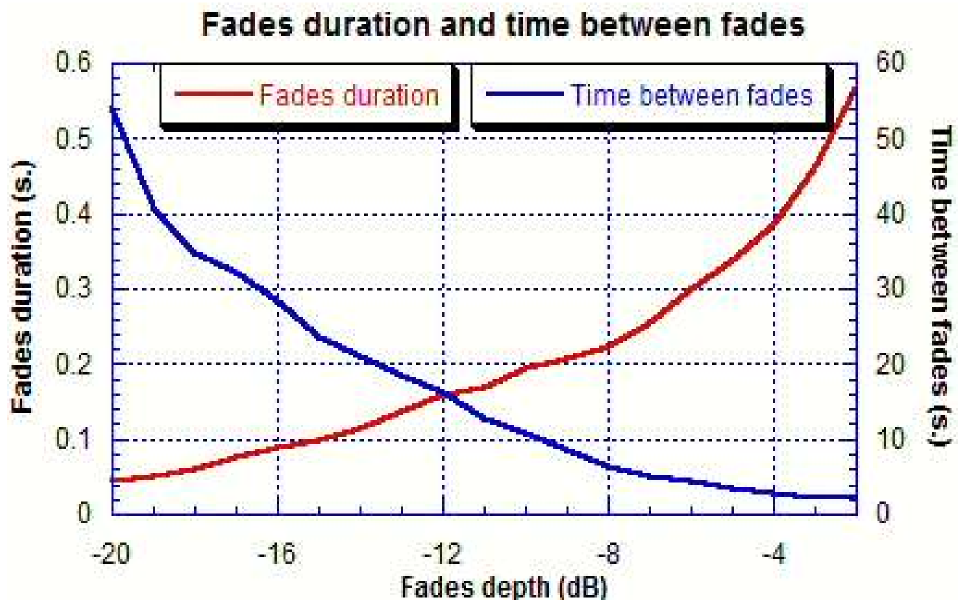

1 hour of data
at a high level of scintillations

Using all data recorded

% of time a fade depth level is exceeded

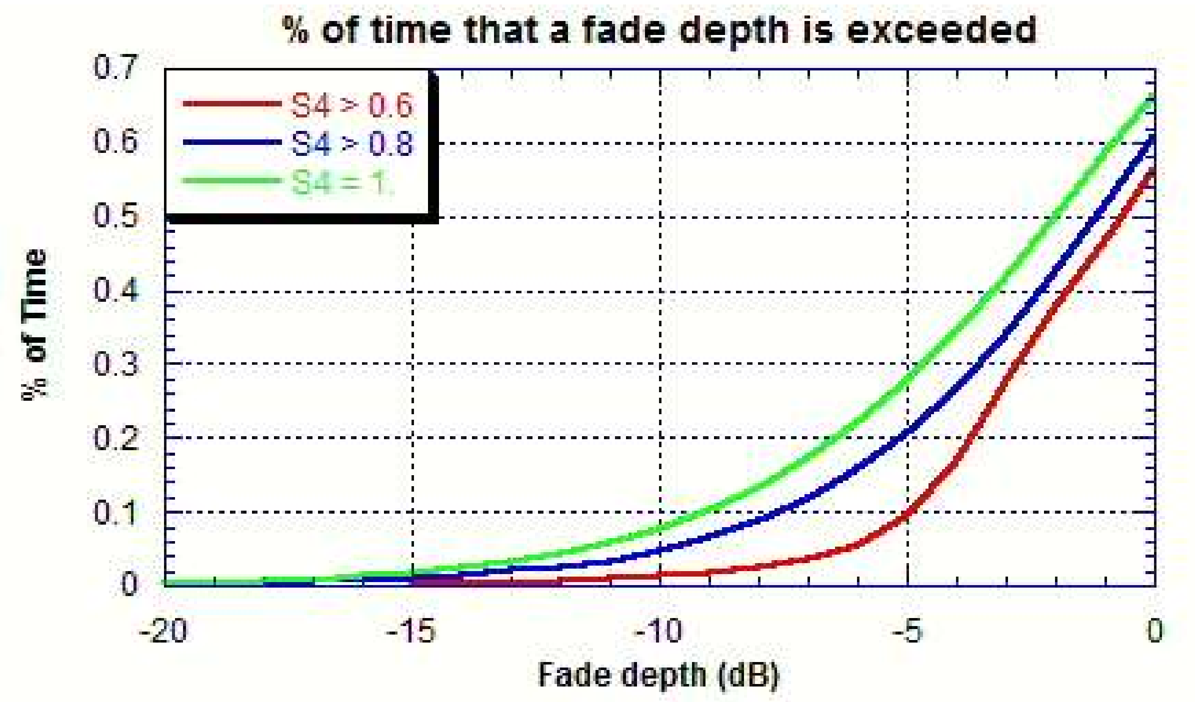

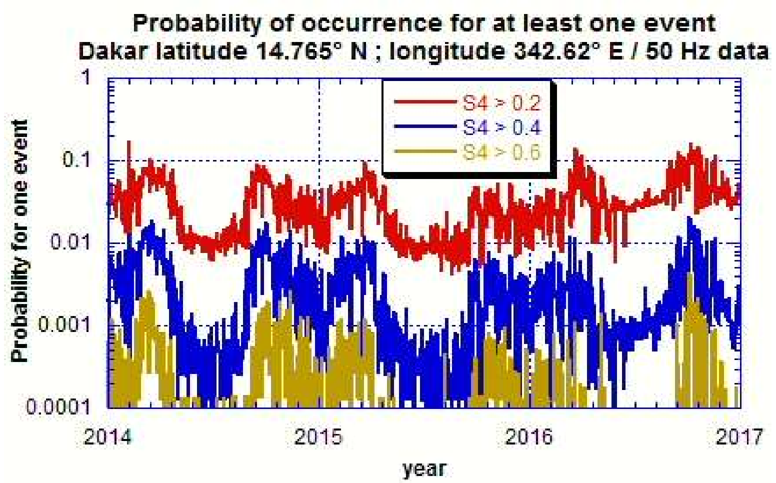

$$P = p(S4) * p(\text{Fade Depth})$$

Time Series
Frequency correlation / Observations
Weak scintillations vs strong scintillations

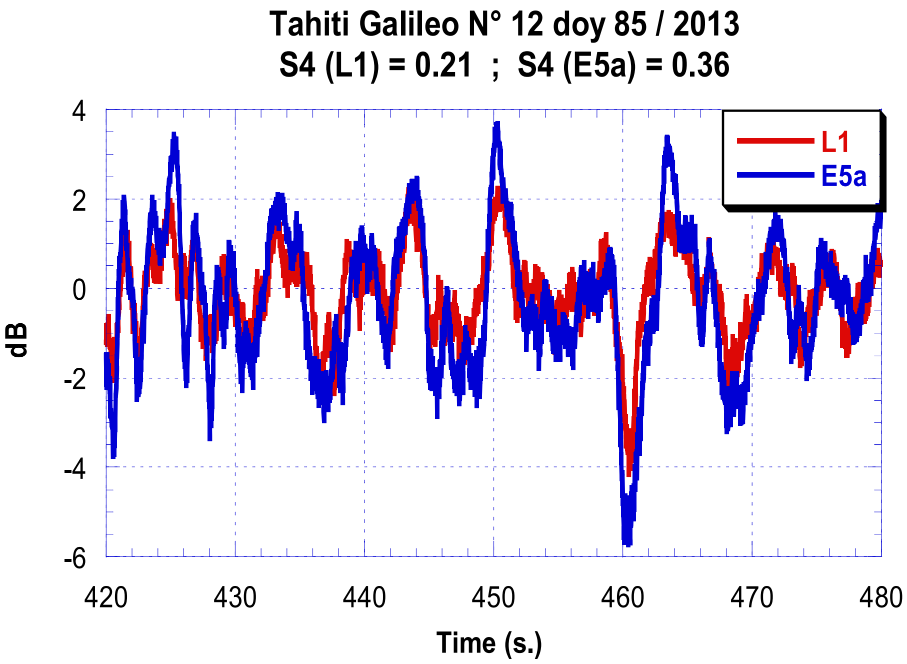

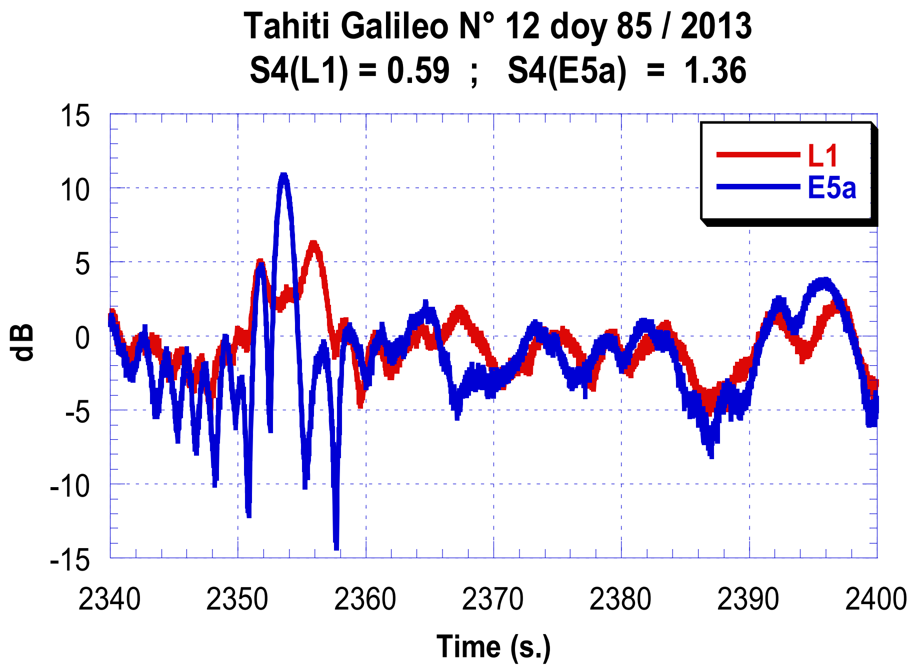

Weak scintillations **Strong scintillations**

Time Series
Frequency Correlation / (Modelling)

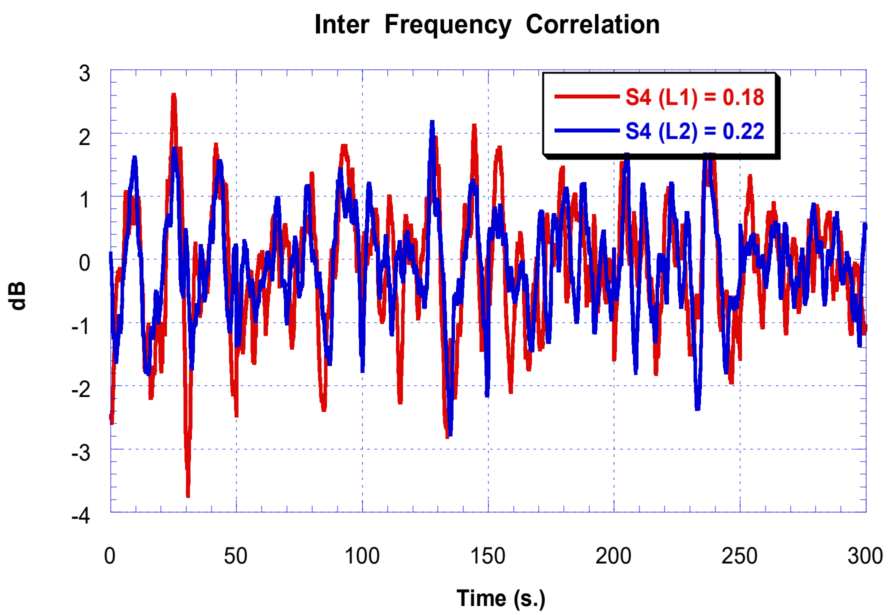

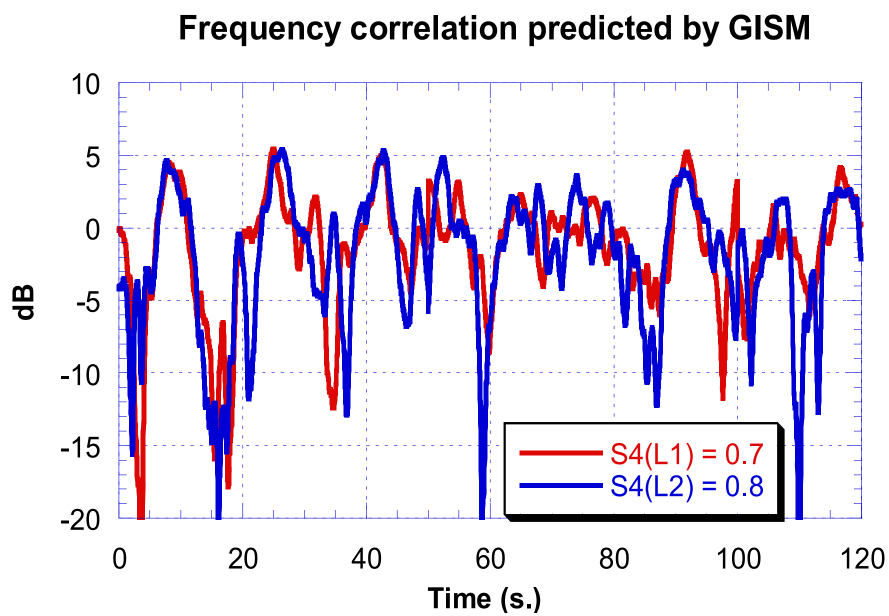

Weak scintillations **Strong scintillations**

Inter Frequency Correlation

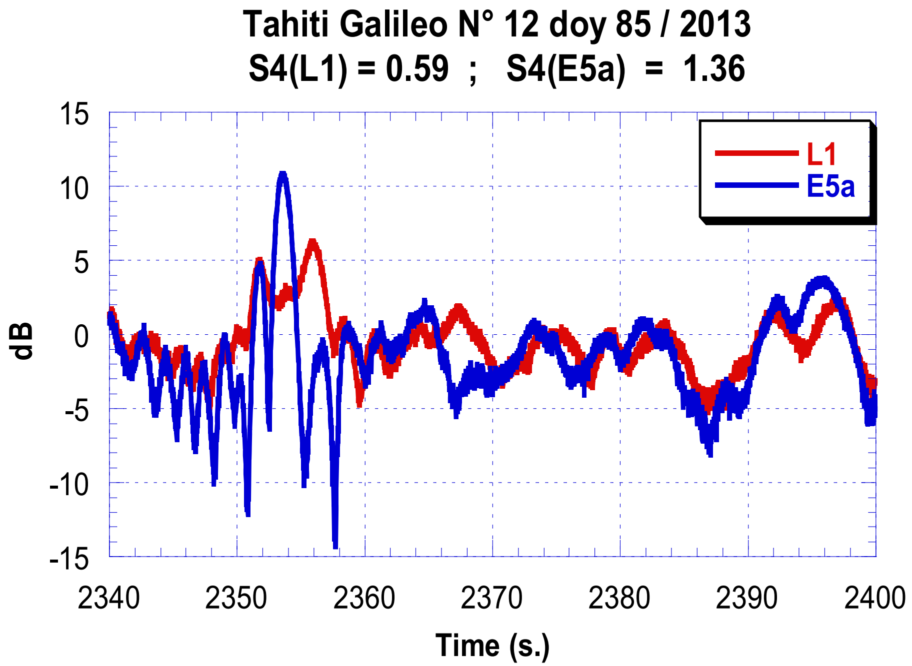

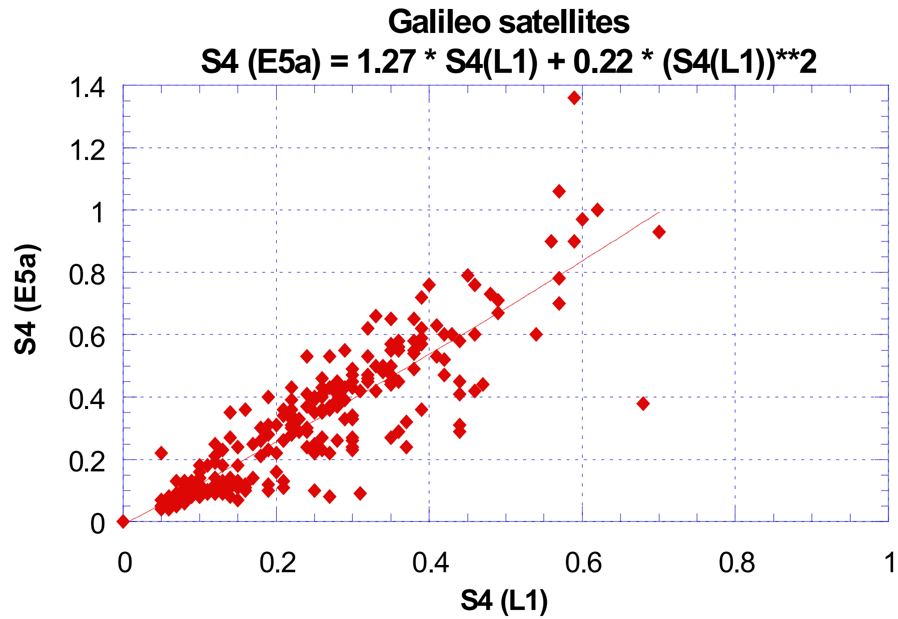

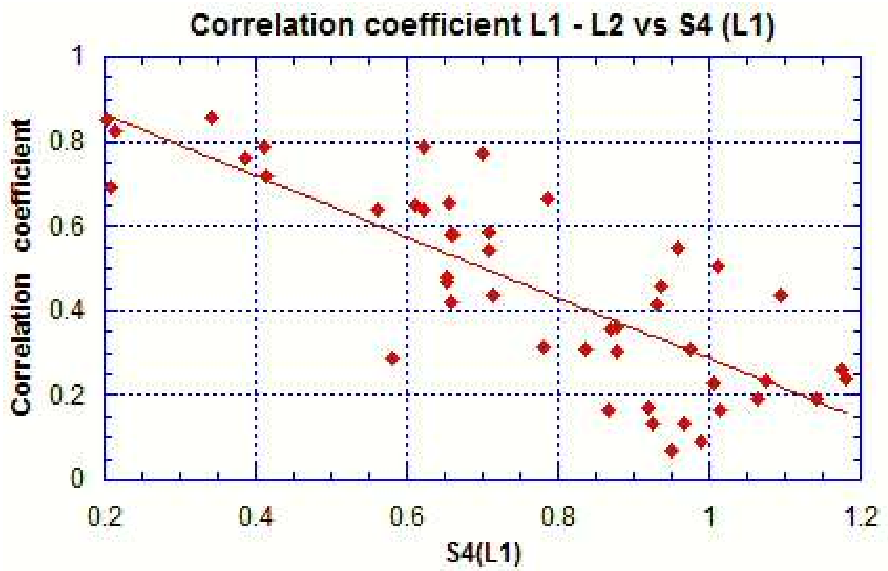

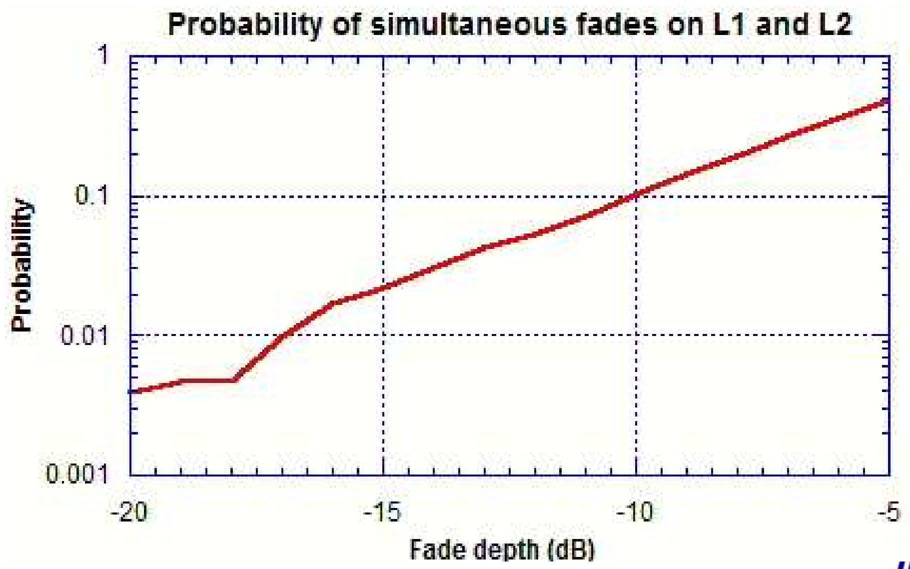

Section 2

Turbulent Ionosphere
The High Latitudes

High Latitude Receivers Network

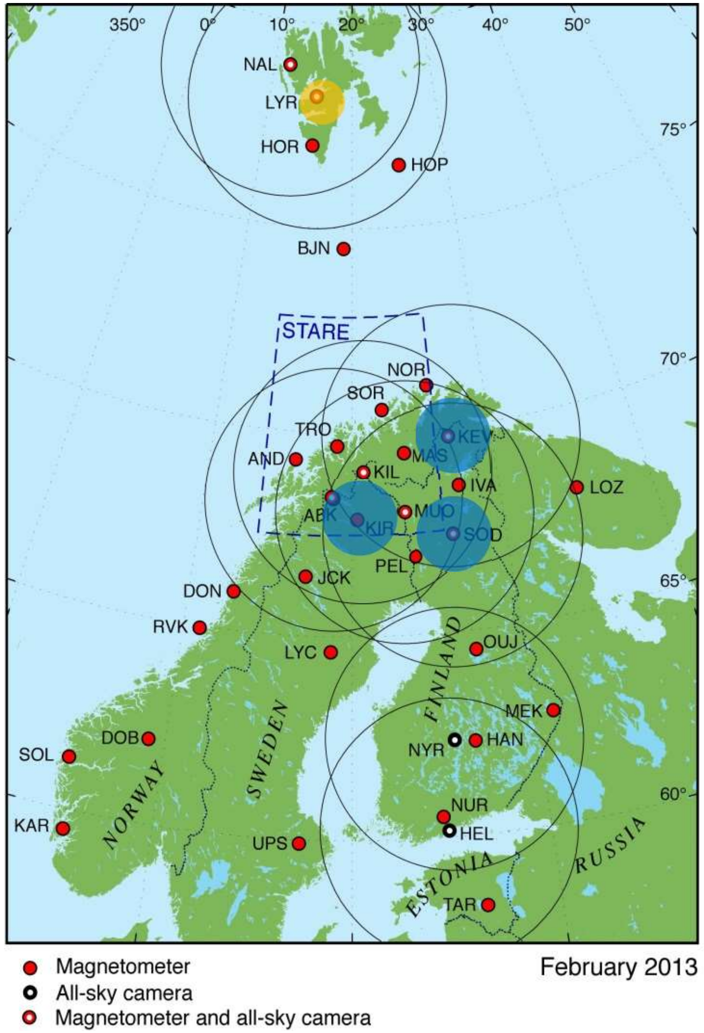

MONITOR site

Station Name	Project	Latitude	Longitude	Equipment	Sampling frequency
Sodankylä (Finland)	Monitor	67.25° N	26.36° E	GSV4004B	50 Hz
Kevo (Finland)	Monitor	69.75°N	27.019° E	GSV4004B	50 Hz
Kiruna (Sweden)	Monitor	67.743° N	21.06° E	PolaRxS	50 Hz

High Latitudes Fluctuations

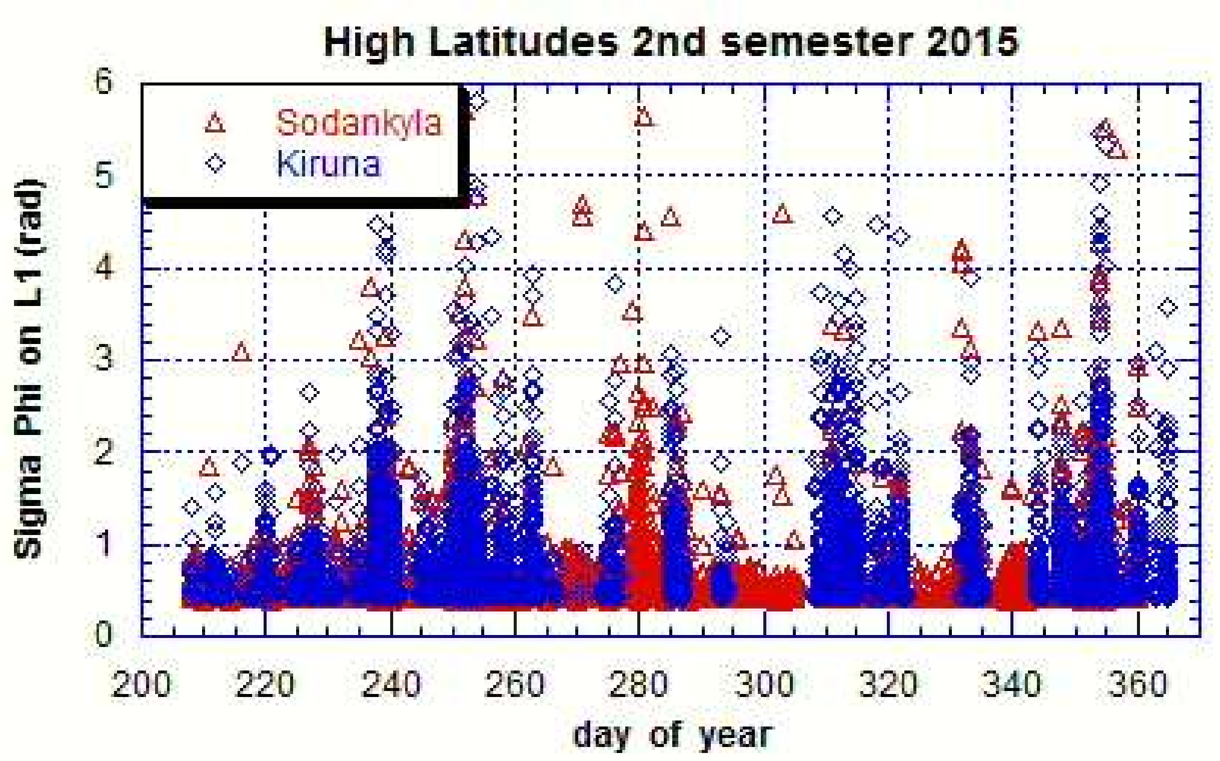

Sodankyla : Novatel GSV 4004B receiver
Kiruna : Septentrio PolaRxS receiver

Distance Sodankyla – Kiruna : 280 km

Relationship Phase fluctuation / AE & Kp Indices High Latitudes

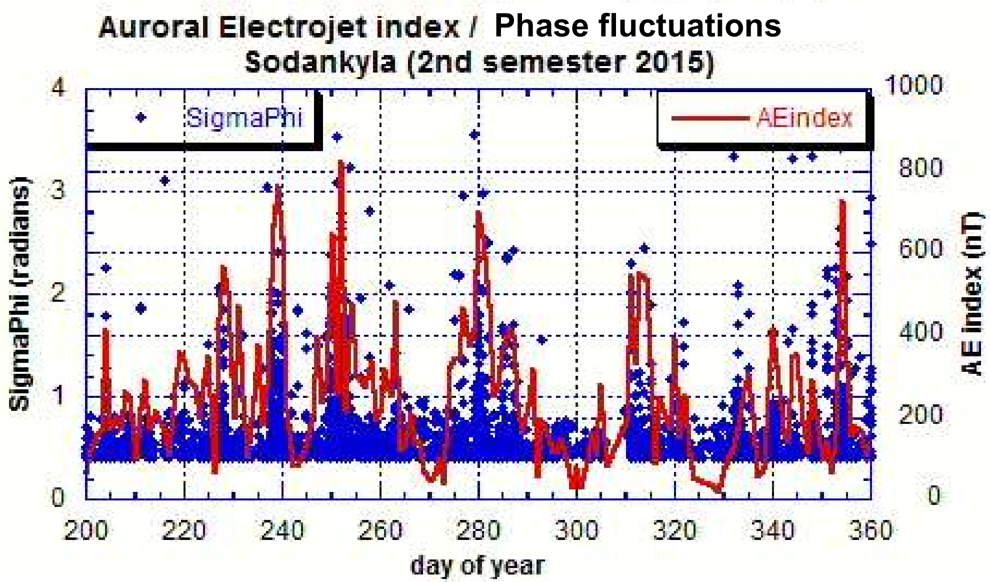

December 2015 magnetic storm

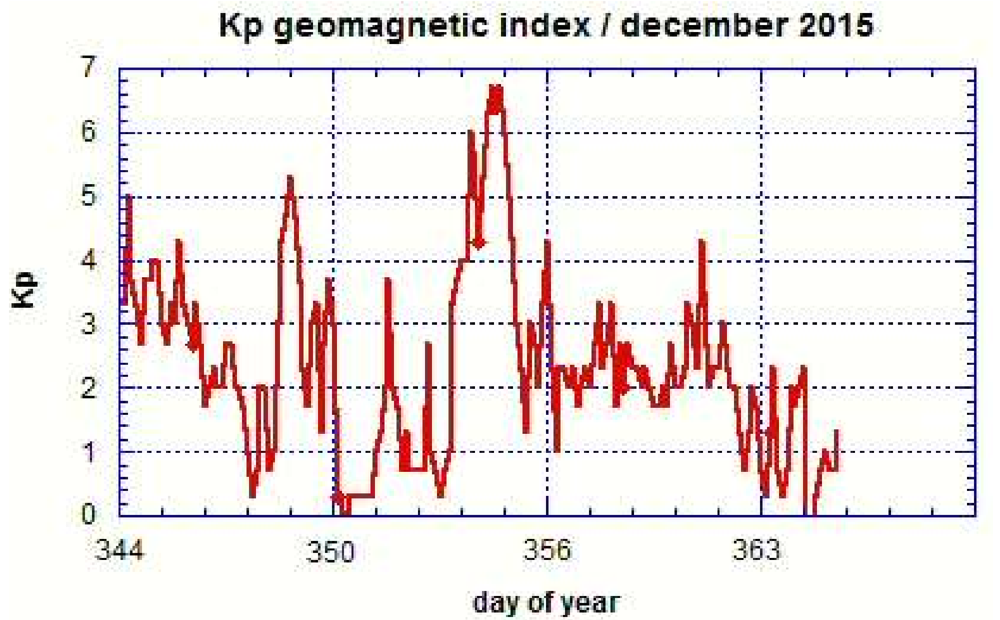

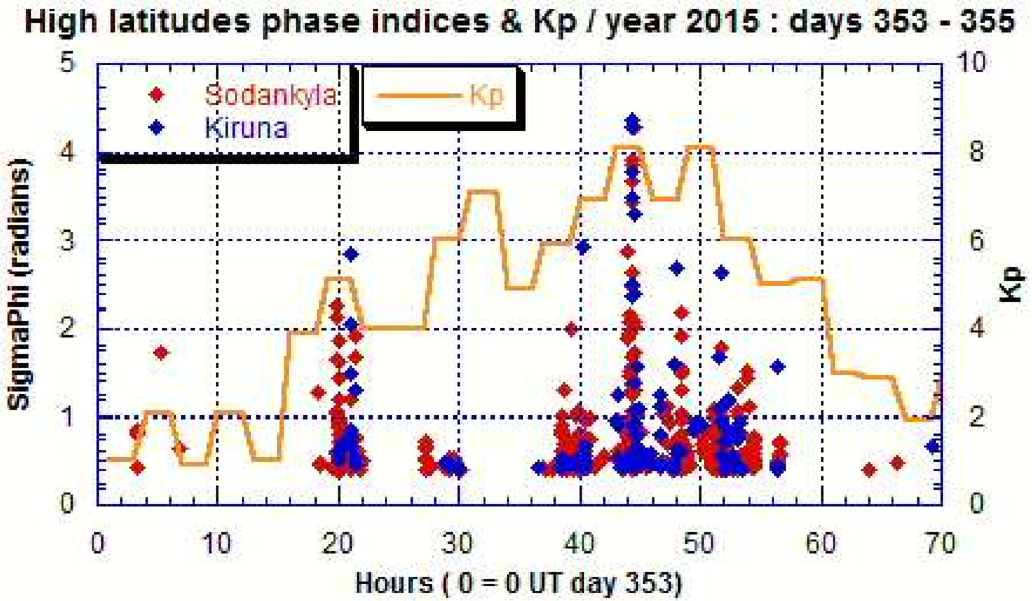

December 2015 Magnetic Storm
Phase fluctuation

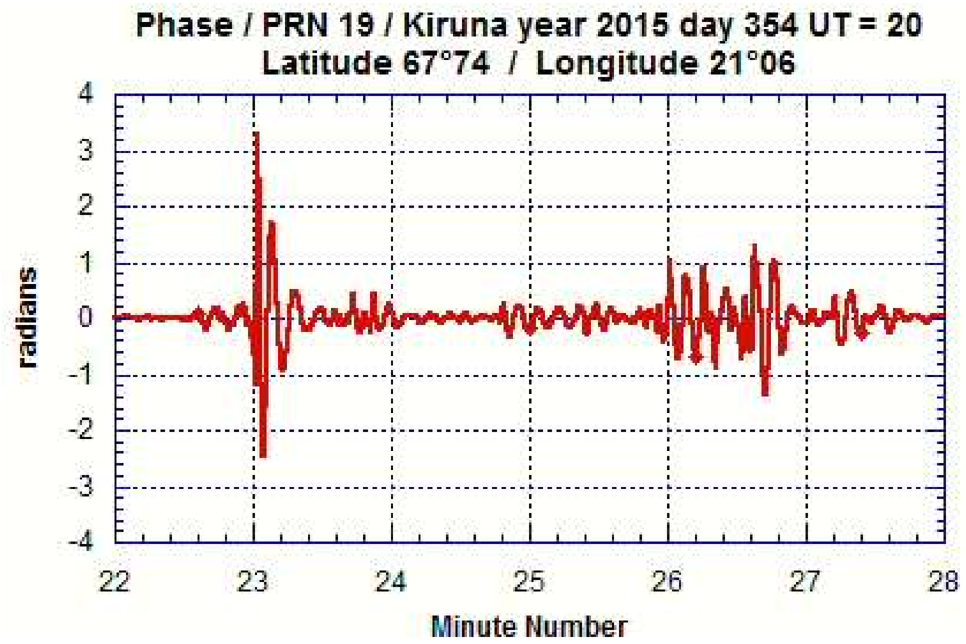

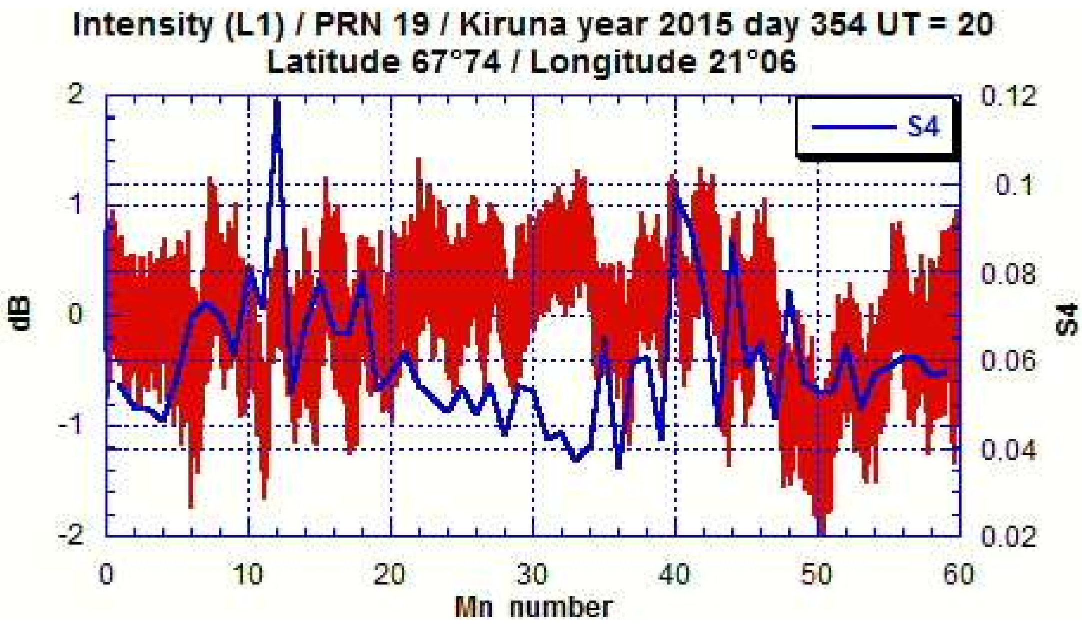

No fluctuations outside these 6 minutes

The intensity fluctuation is not an issue for a GNSS application

Receiver : PolaRxS Septentrio

High latitude fluctuations

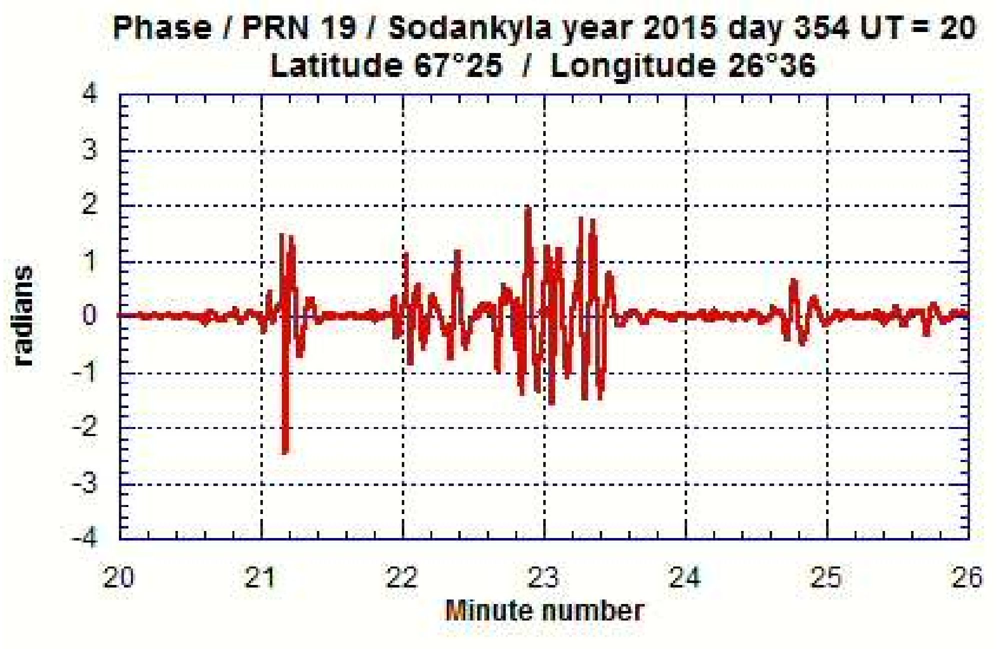

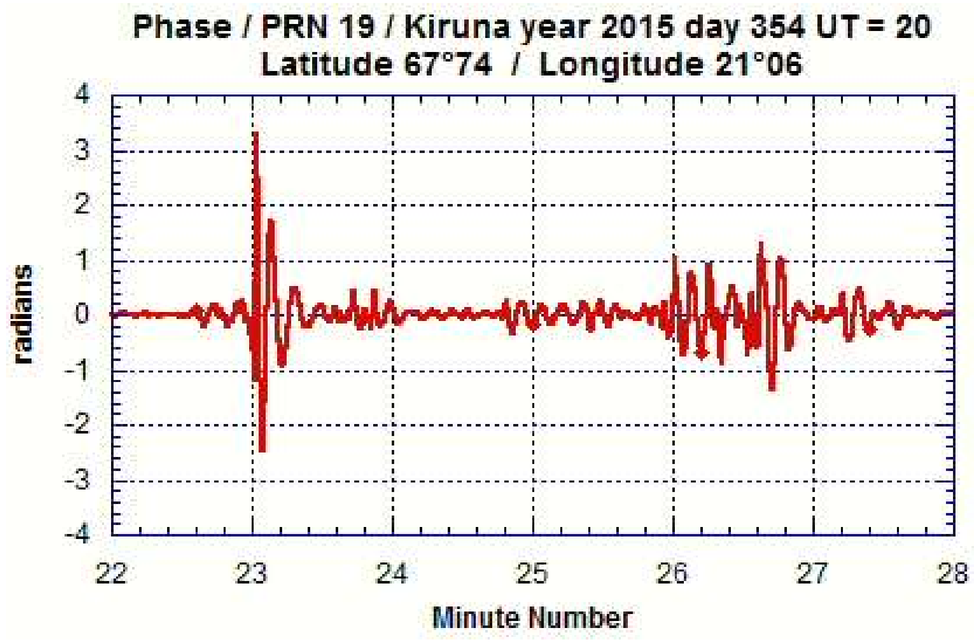

Sodankyla **Kiruna**

Distance between receivers : 280 km
Drift velocity : around 2 km / s. westward

→ **Refraction rather than diffraction**

Fluctuations spectra : High Latitudes vs Low Latitudes

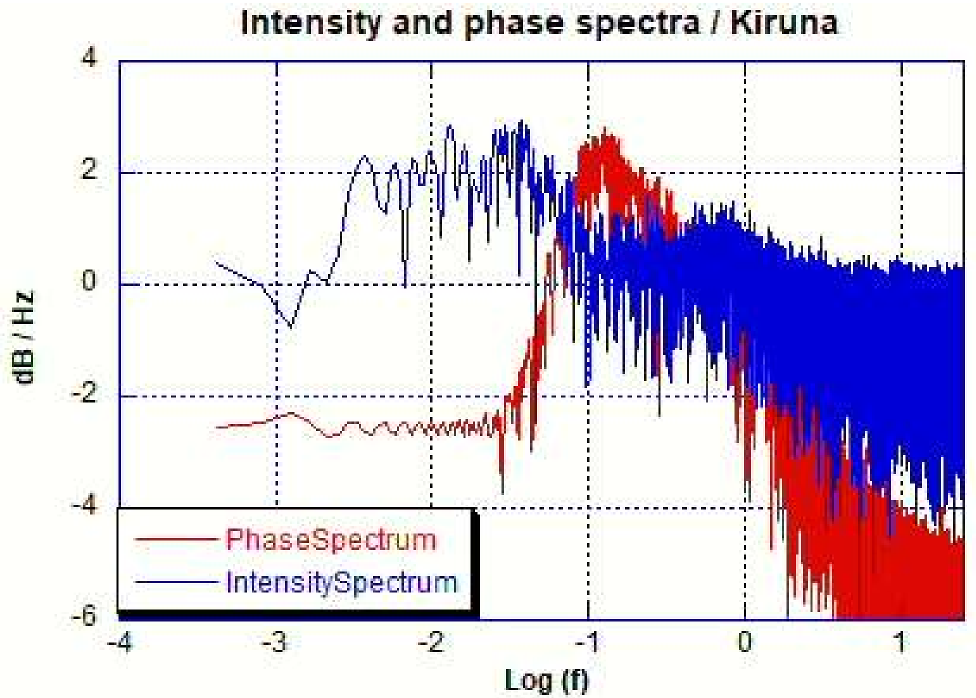

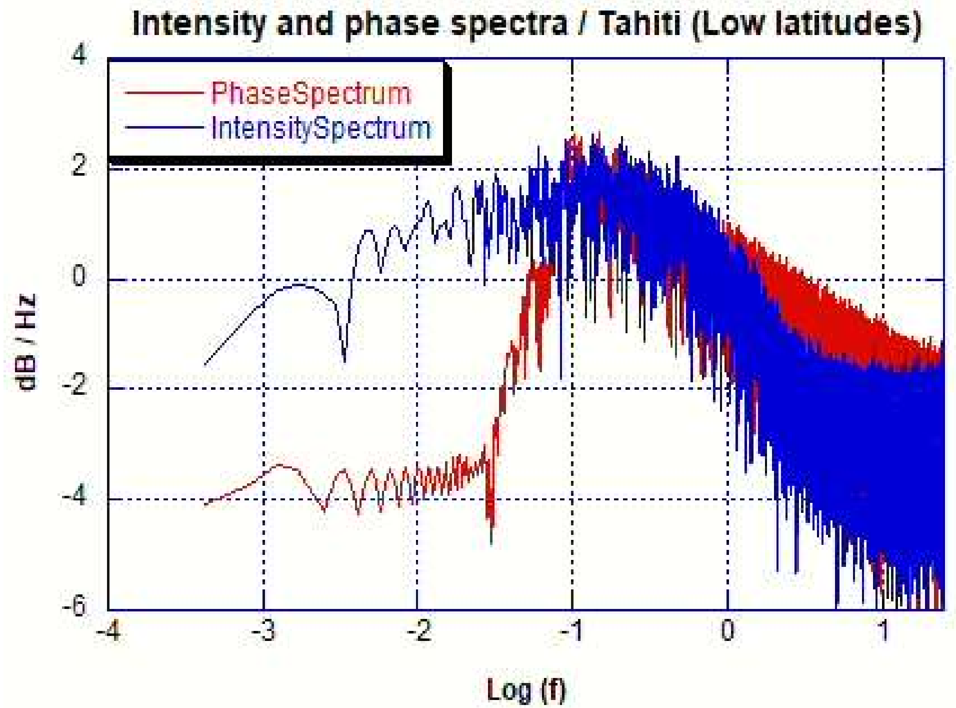

High frequencies → Low frequency content

Different parameters for the Fresnel size, the focal scale and the altitude of inhomogeneities

Sigma Phi & ROTI High Lat

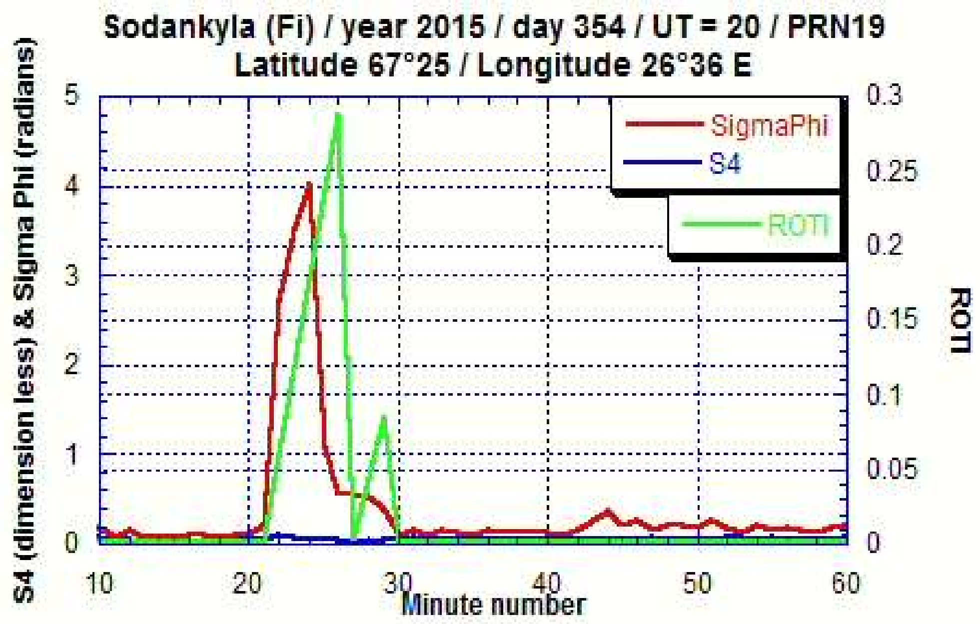

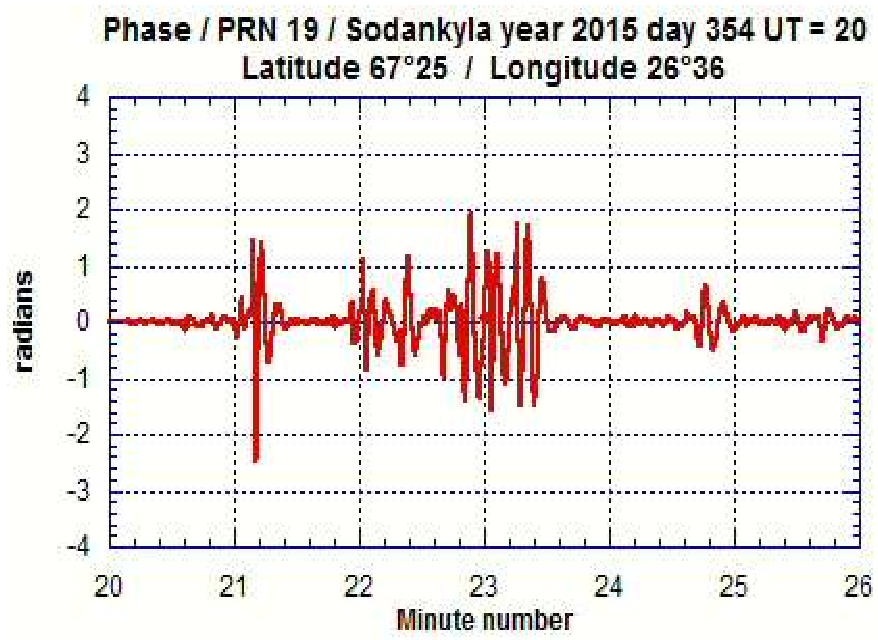

(Relationship of fluctuations to the ROTI index and consequently to TEC gradients)

Probability of occurrence

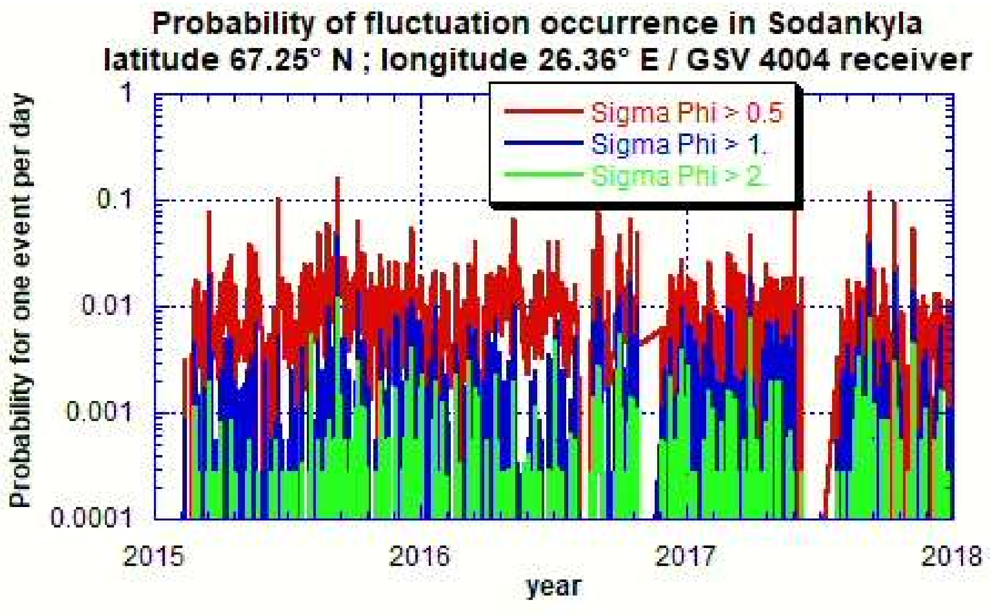

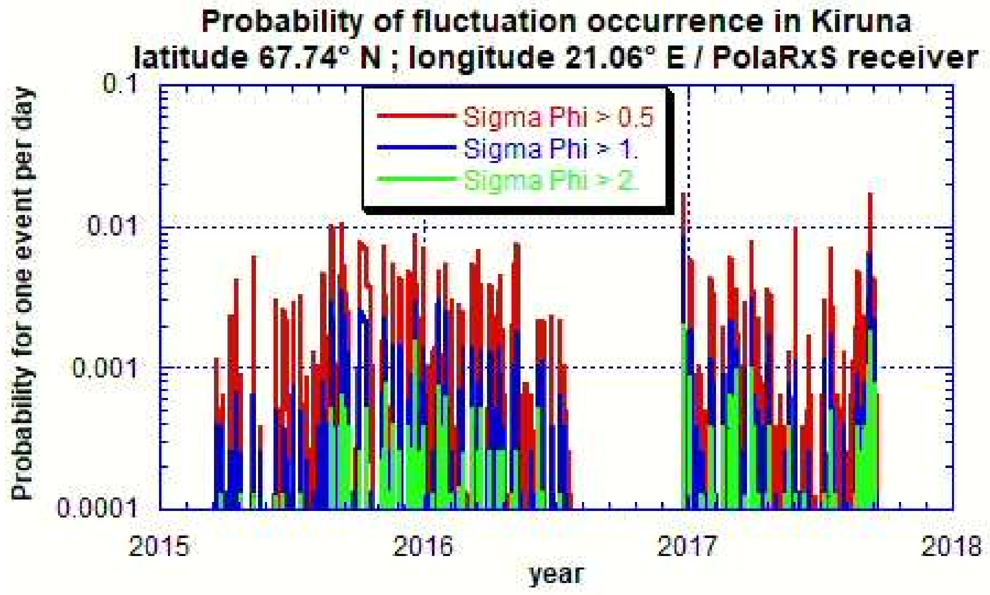

GSV4004B receiver **PolaRxS receiver**

1 order of magnitude lower with the PolaRxS receiver

How many links at the same time

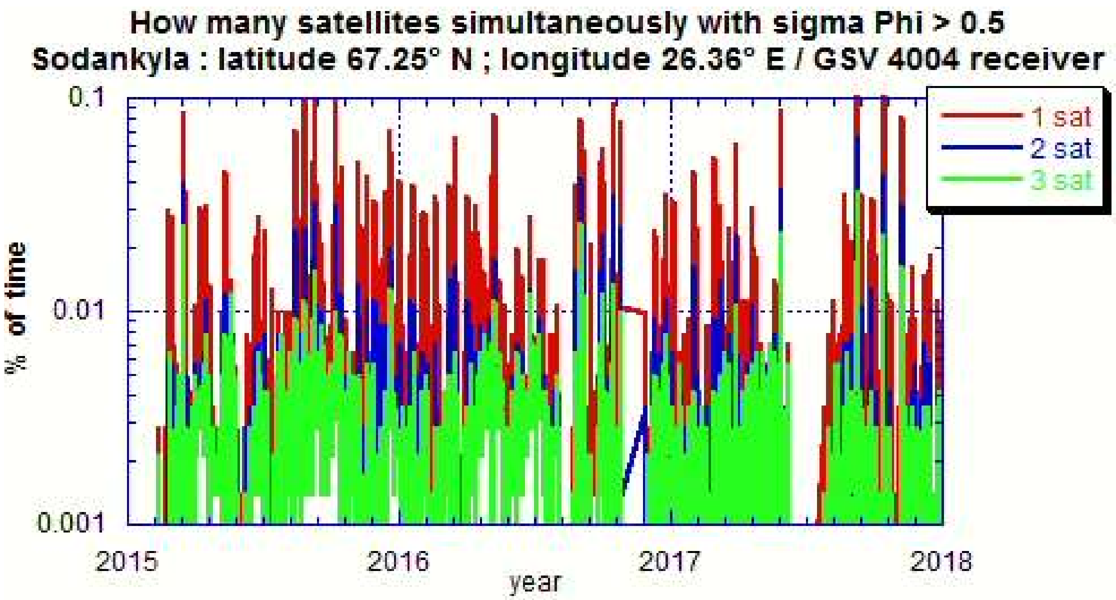

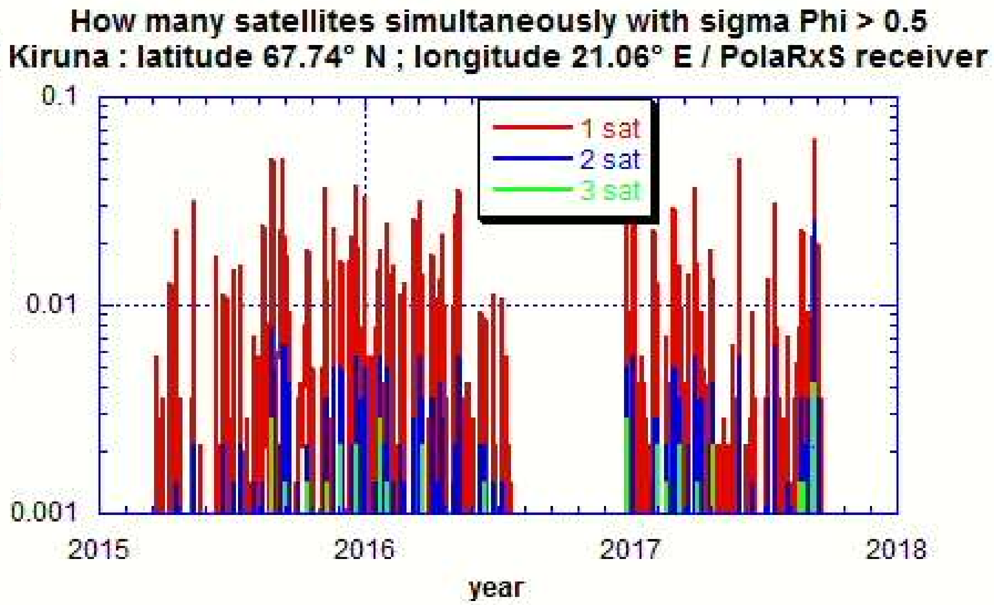

GSV4004B receiver

PolaRxS receiver

The % of time is lower with the PolaRxS receiver

High Latitudes Number of Links

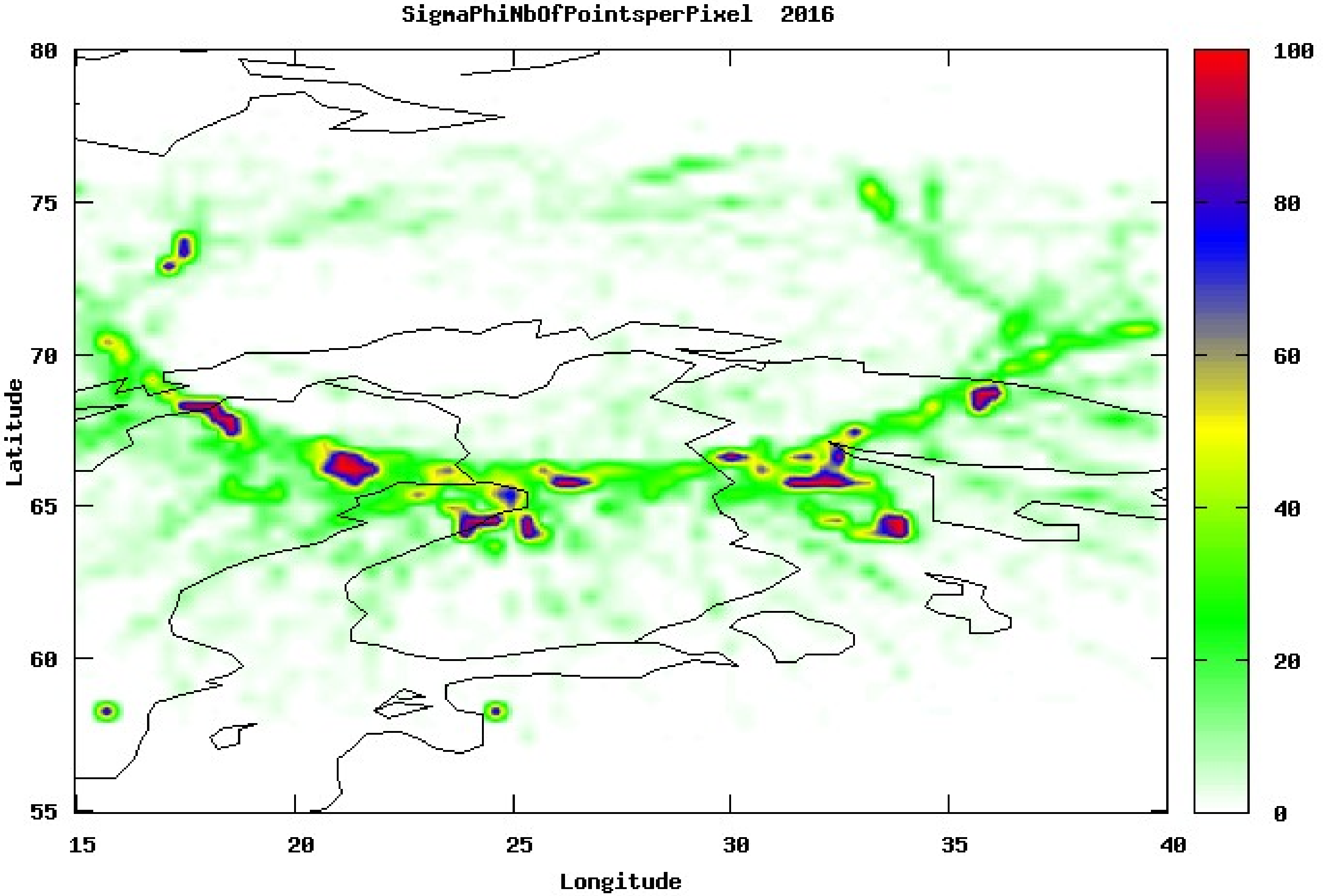

Peak value at about 65° of latitude

Fluctuations Map / High Latitudes

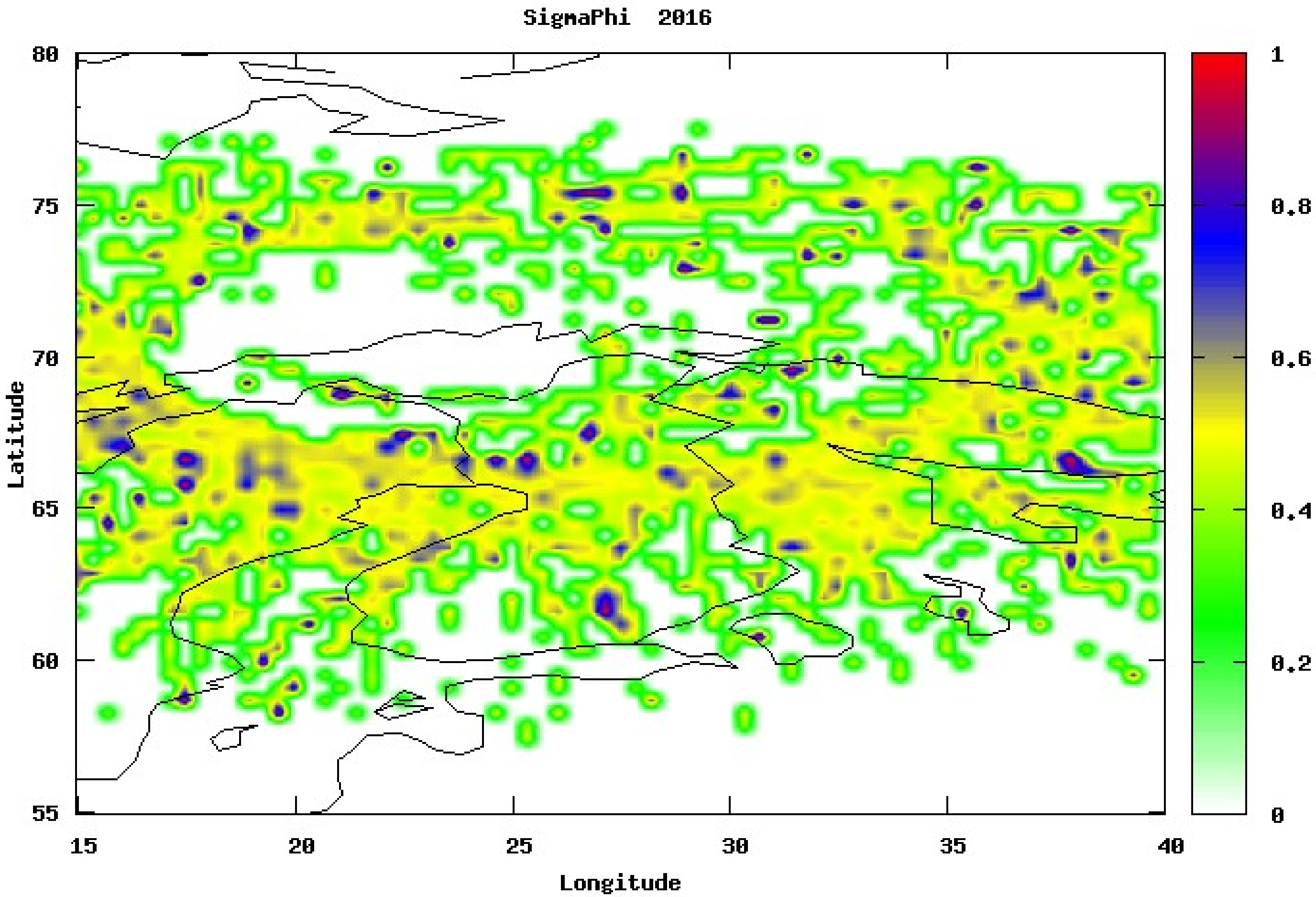

Scandinavian sector

sigma phi median values at IPPs cumulated over the year

Cycle Slips
Low Latitudes vs High Latitudes

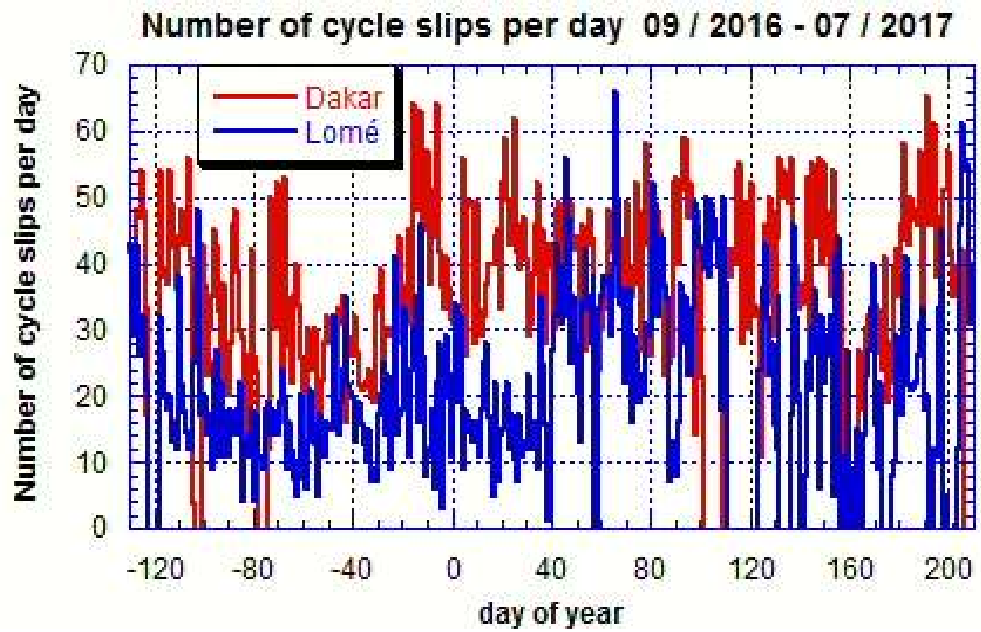

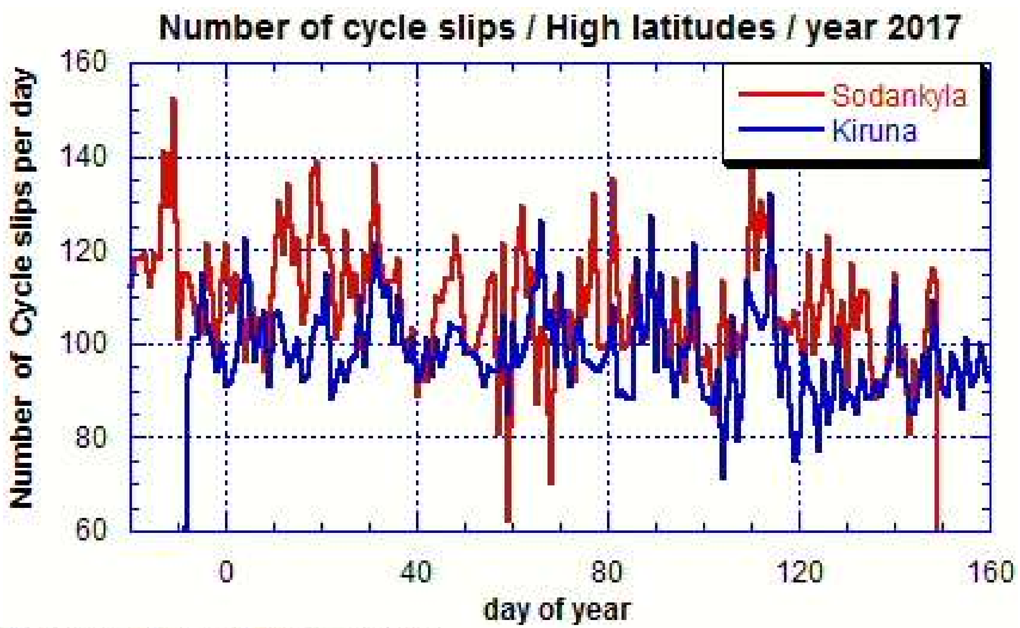

Rinex input data files
(1 Hz)

Blewit algorithm

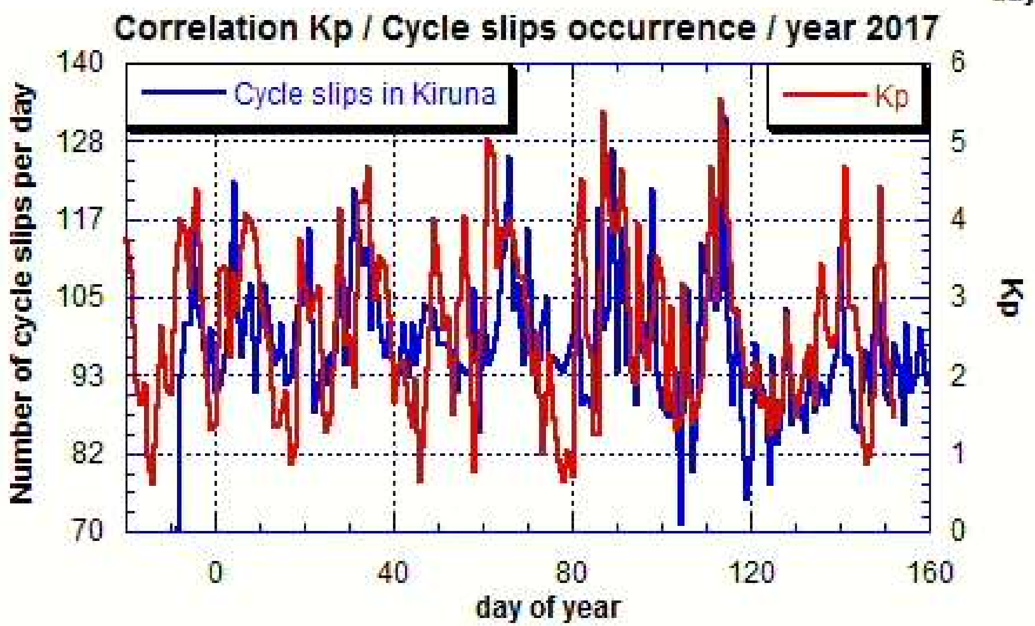

Section 3

Modelling

Multiple Phase screens technique
GISM*

* developed under ESA / ESTEC contract

Béniguel Y., P. Hamel, “A Global Ionosphere Scintillation Propagation Model for Equatorial Regions”, Journal of Space Weather Space Climate, 1, (2011), doi: 10.1051/swsc/2011004

Ray Technique

Appleton Hartree formula

$$n^2 = 1 - \frac{X}{U - \frac{Y^2 \sin^2\vartheta}{2(U-X)} \pm \left[\frac{Y^4 \sin^4 \vartheta}{4(U-X)^2} + Y^2 \cos^2\vartheta \right]^{1/2}} \approx 1 - X$$

$X = (f_P / f)^2$ and $f_P = 9\sqrt{N_e}$ is the plasma frequency

$Y = f_b / f$ and $\omega_b = eB/m$ f_b is the gyro frequency

$U = 1 - jZ$ and $Z = \upsilon / \omega$ is the collision frequency

Line of sight calculation

$$\frac{dx_i}{dt} = \frac{c^2 k_i}{\omega} \qquad \frac{dk_j}{dt} = -\frac{\omega_P}{\omega}$$

Runge Kutta algorithm ; NeQuick model for Ne

Mean Errors

distance	phase	Faraday rotation
$\Delta L = \frac{40.3\, N_T}{f^2}$ with $N_T = \int_0^z N_e\, ds$	$\Delta \Phi = k \int_0^{\Delta z} \Delta n(\rho, z)\, dz = \lambda\, r_e\, N_T$	$\Psi = \frac{e^3}{2\varepsilon_0\, c\, m^2\, \omega^2} \int_0^z N_e\, B \cos\vartheta\, ds$

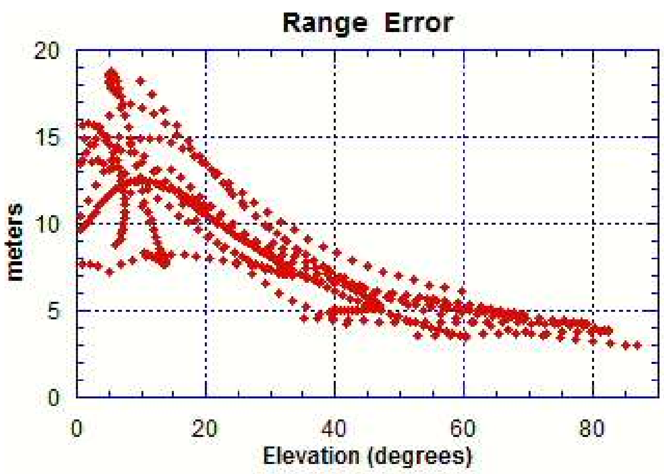

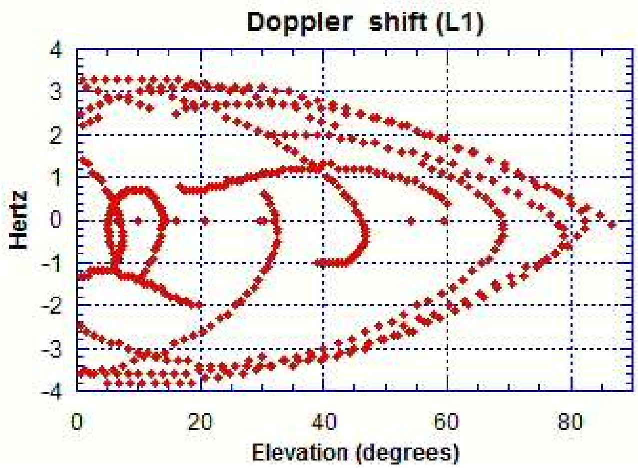

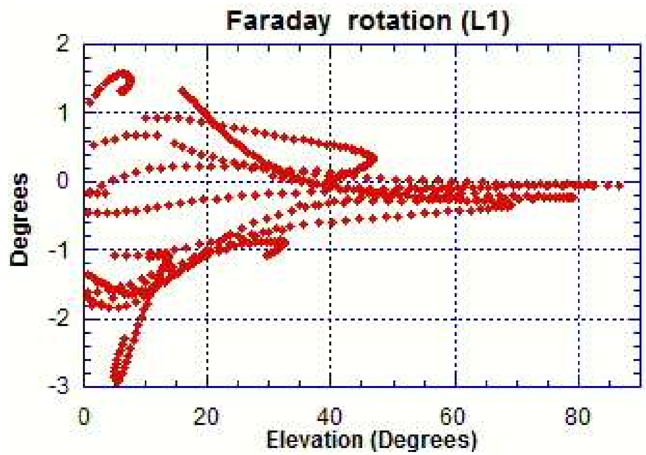

Mid latitudes / solar flux 150

HF Propagation

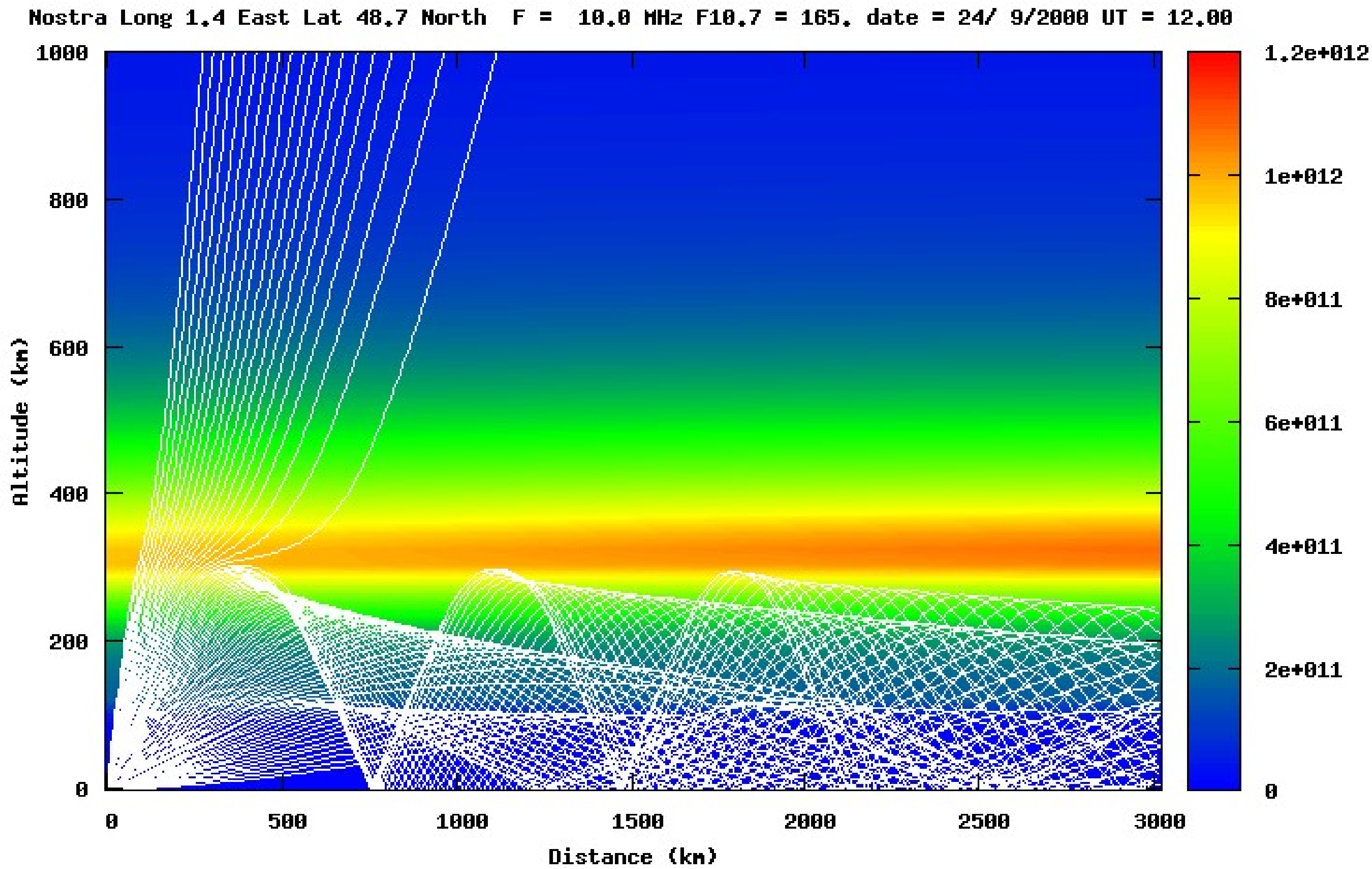

2 reflexion heights (caustics of reflected rays) at D & E layers

Field Propagation Equation

$$E(\rho, z, \omega, t) = U(\rho, z, \omega) \exp\left\{ j\left(\omega t - \int \left\langle k(z') \right\rangle dz' \right) \right\}$$

The field amplitude value U is a solution of the parabolic equation (paraxial approximation)

$$2jk \frac{\partial U(\rho)}{\partial z} + \nabla_t^2 U(\rho) + k^2 \varepsilon_1(\rho) U(\rho) = 0$$

Method of solution : phase screen technique

Field Propagation Equation

Solution of the parabolic equation

$$2jk\frac{\partial}{\partial z}\langle U(r)\rangle + \nabla_t^2\langle U(r)\rangle + k^2\langle \varepsilon(r)\, U(r)\rangle = 0$$

$$2jk\frac{\partial}{\partial z}\langle U(r)\rangle + \nabla_t^2\langle U(r)\rangle + j\,\frac{k^3}{4}\,A(0)\,\langle U(r)\rangle = 0$$

Using the medium index autocorrelation function

$$B(z,\rho) = \langle \varepsilon(\rho_1)\;\varepsilon(\rho_2)\rangle \qquad A(\rho) = \int B(z,\rho)\,dz$$

Phase Screen Technique

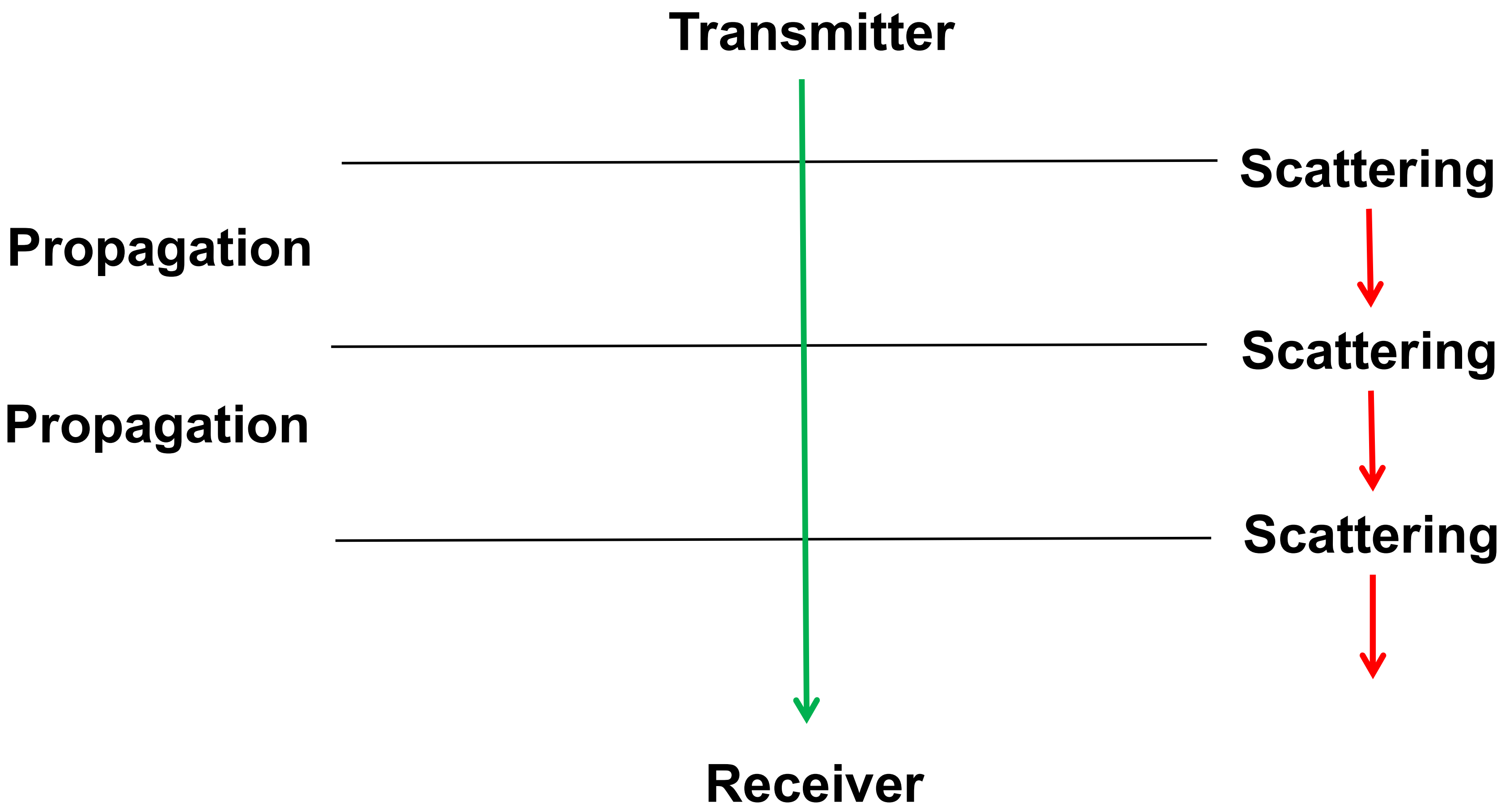

Propagation : 1st & 3rd terms ; scattering : 2^{nd} & 3rd terms

Phase & Intensity Spectra

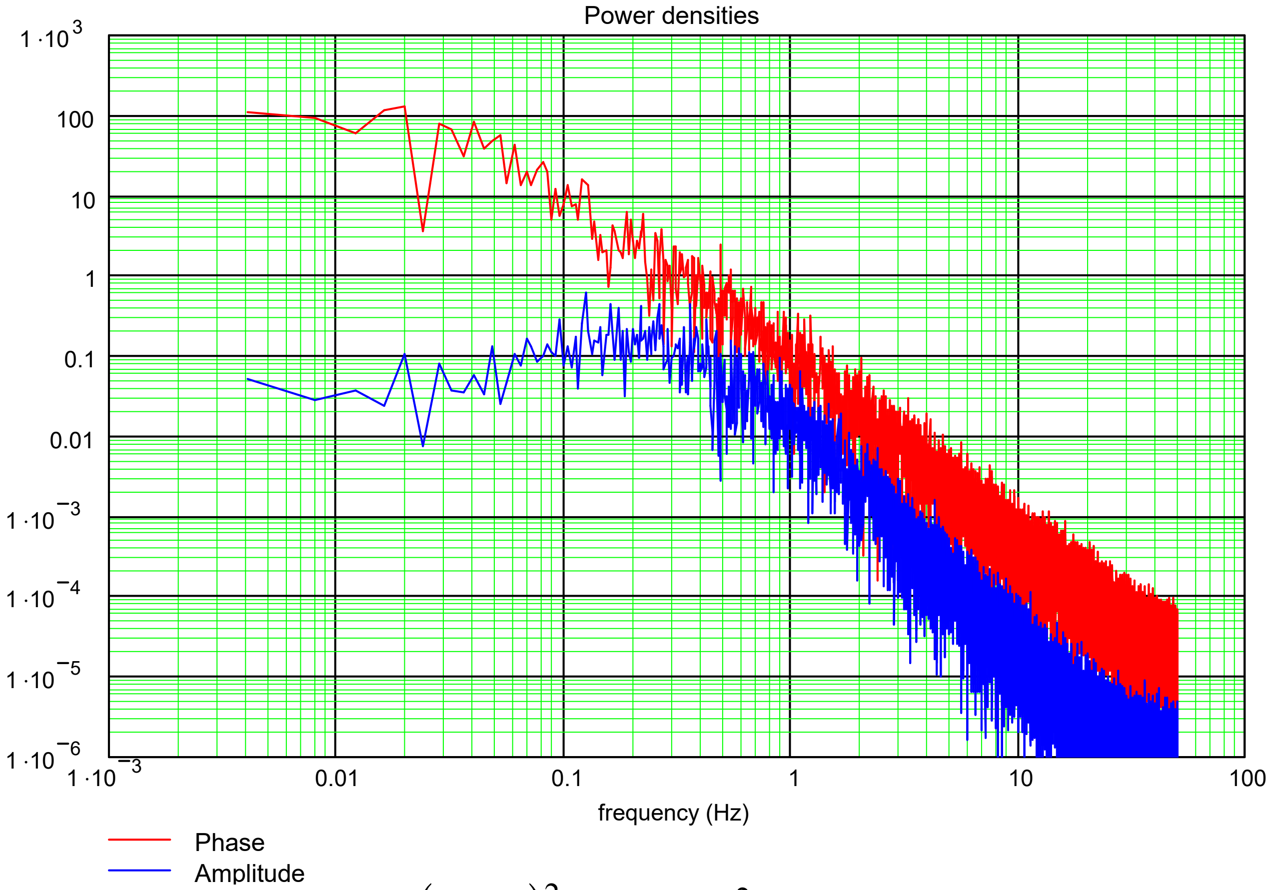

$$\gamma_{\Phi}(K) = \frac{(\lambda r_e)^2 \, L \, C_S \, \sigma_{Ne}^2}{\left(K^2 + q_0^2\right)^{p/2}} = \frac{C_P}{\left(K^2 + q_0^2\right)^{p/2}}$$

3 parameters : σ_{Ne} ; q_0 ; p

Phase Synthesis (1D)

$$\Phi(\rho) = \mathrm{FFT}^{-1}\left(\mathrm{FFT}(u) * \gamma_{\Phi}(k)\right)$$

u random number with a uniform spectral density

Done at each successive layer

1D Analysis
Isotropic Medium

$$B_{\Phi}(\rho) = \frac{C_P}{2\pi}\int \gamma_{\Phi}(k)\,\exp(-jk\rho)\,dk$$

$$\left[B_{\Phi}(\rho)\right]_{1D} = \frac{C_P}{2\pi}\,\frac{\sqrt{\pi}}{2^{(p-3)/2}\,\Gamma(p/2)}\,q_0^{1-p}\,(\rho q_0)^{(p-1)/2}\,K_{(p-1)/2}(\rho q_0)$$

Anisotropic vs Isotropic

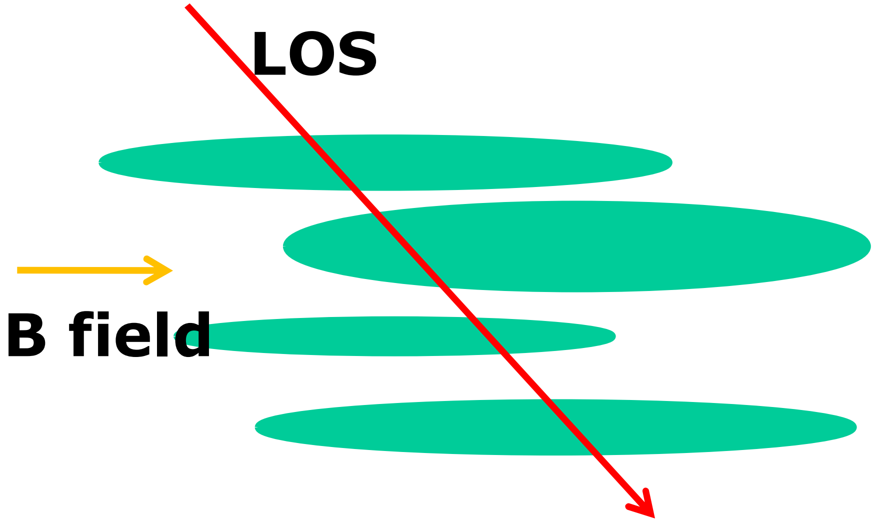

$$\gamma_\Phi(K) = \frac{(\lambda r_e)^2 L C_S \sigma_{Ne}^2 a b}{\left(q^2 + q_0^2\right)^{p/2}}$$

$$\gamma_\Phi(K) = \frac{a b C_P}{\left(\left(AK_{x\perp}^2 + BK_{x\perp} q_{y\perp} + CK_{y\perp}^2\right)^2 + q_0^2\right)^{p/2}}$$

Additional geometric factor* with respect to the 2D case

$$G = \frac{ab}{\left(AC - B^2/4\right)^{1/2}}$$

a, b ellipses axes

A, B, C trigonometric terms resulting from rotations related to variable changes

* Rino CL. 2011. The theory of scintillation with applications in remote sensing. Wiley, New Jersey.

NICT Model : Bubbles Development

- Receiver at d = 180 km
- Satellite at h = 1200 km from d = 350 km to 0 km

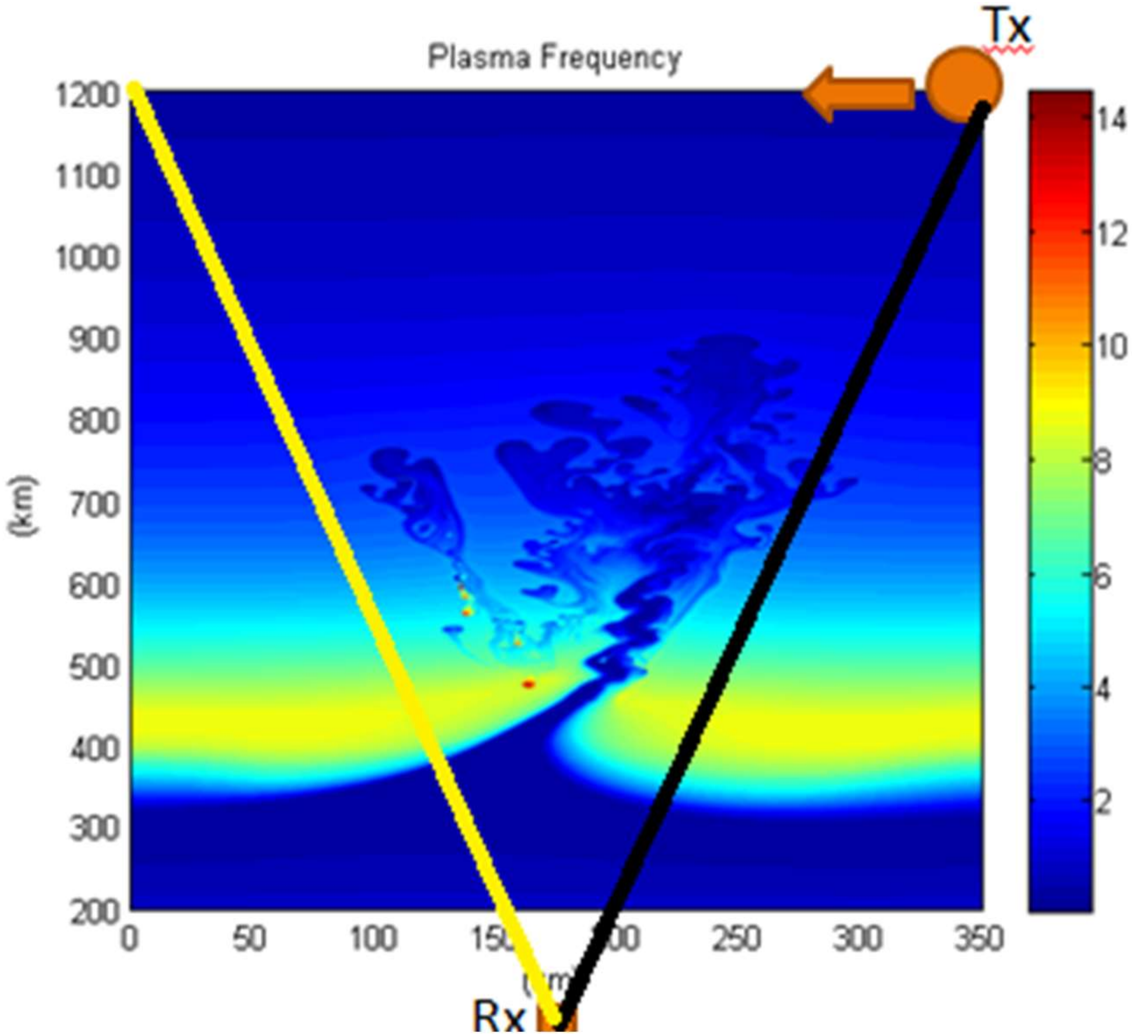

Crossing Bubbles for one Particular Elevation Angle

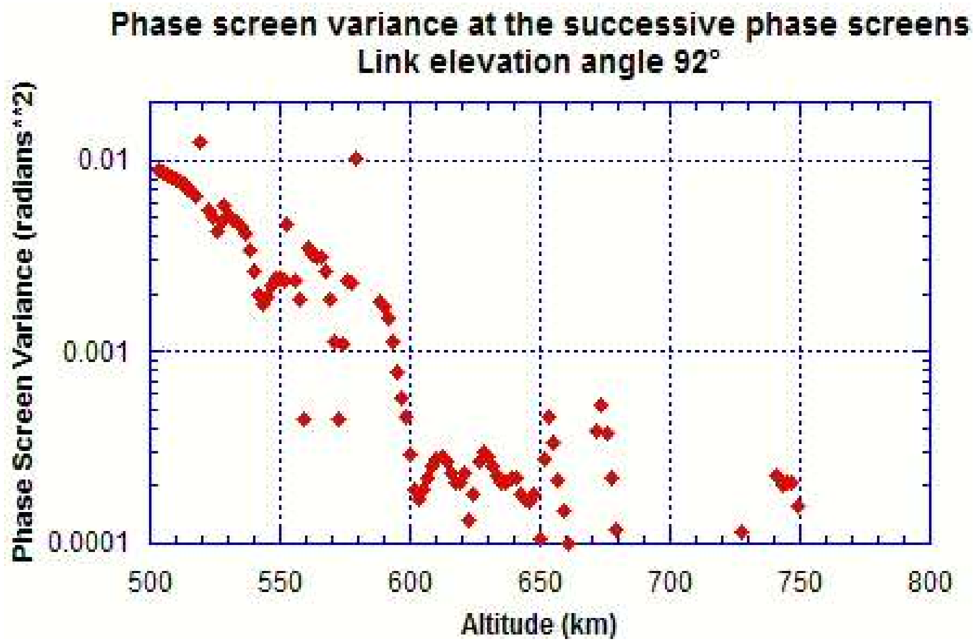

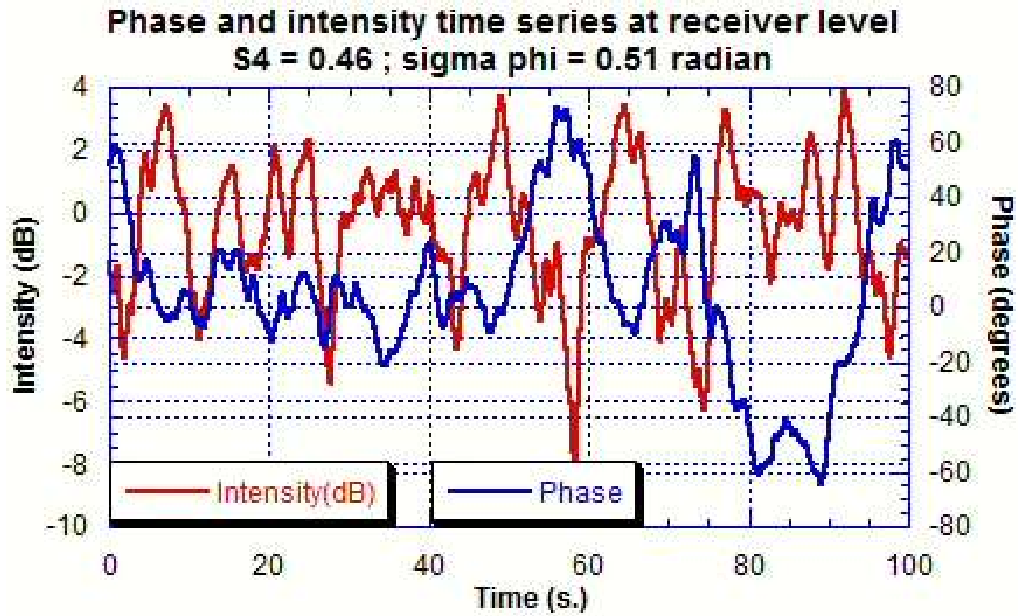

143 phase screens

TEC, S4 and σ_ϕ Time series
Scanning the medium

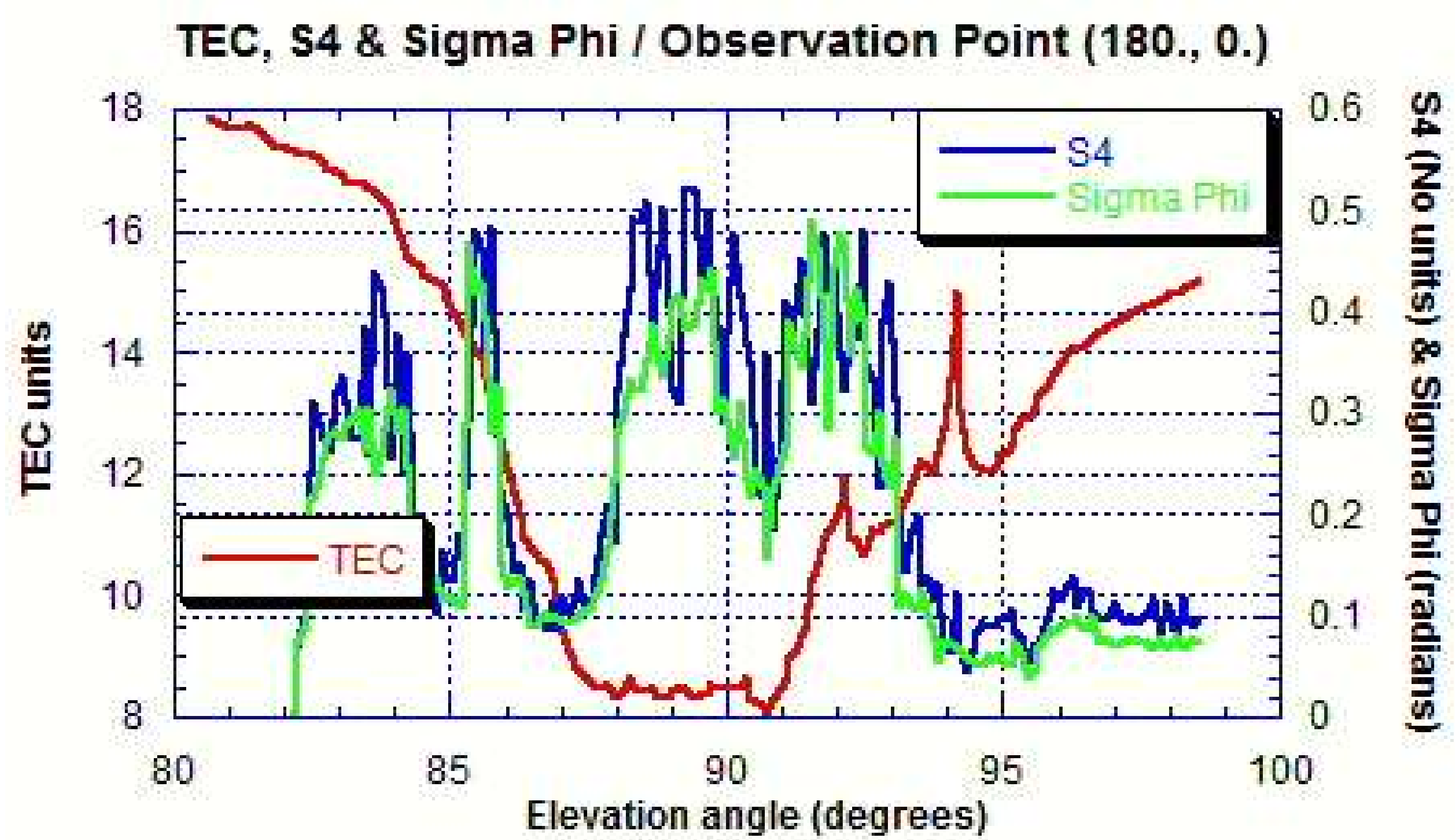

Modelling vs Measurements

Modelling vs Measurements (Intensity of received signal)

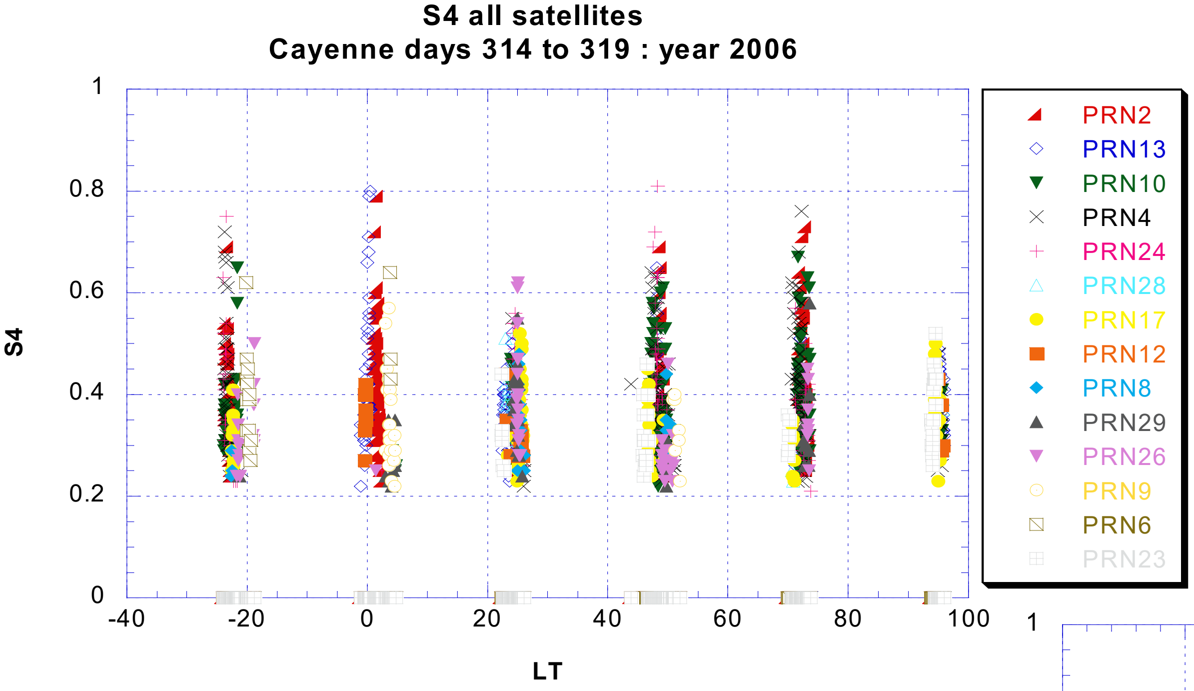

Measurements

Modelling

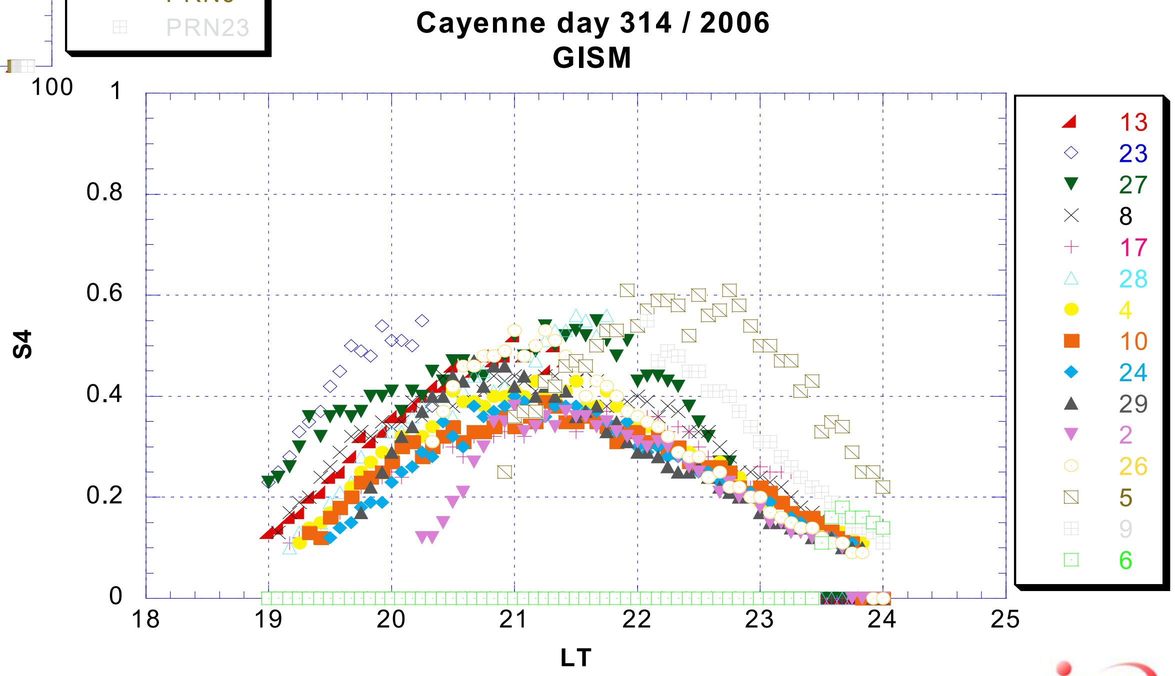

Modelling vs Measurements (Phase of received signal)

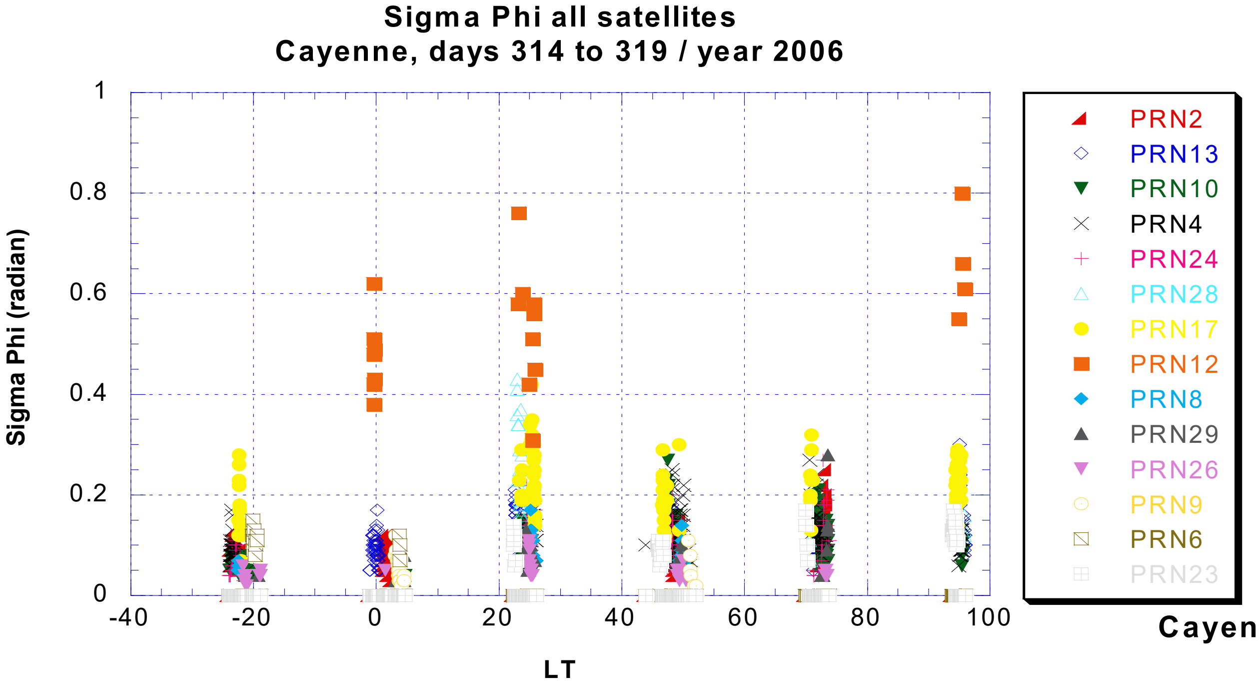

The phase RMS value is slightly lower than the S4 value

← **Measurements**

Modelling →

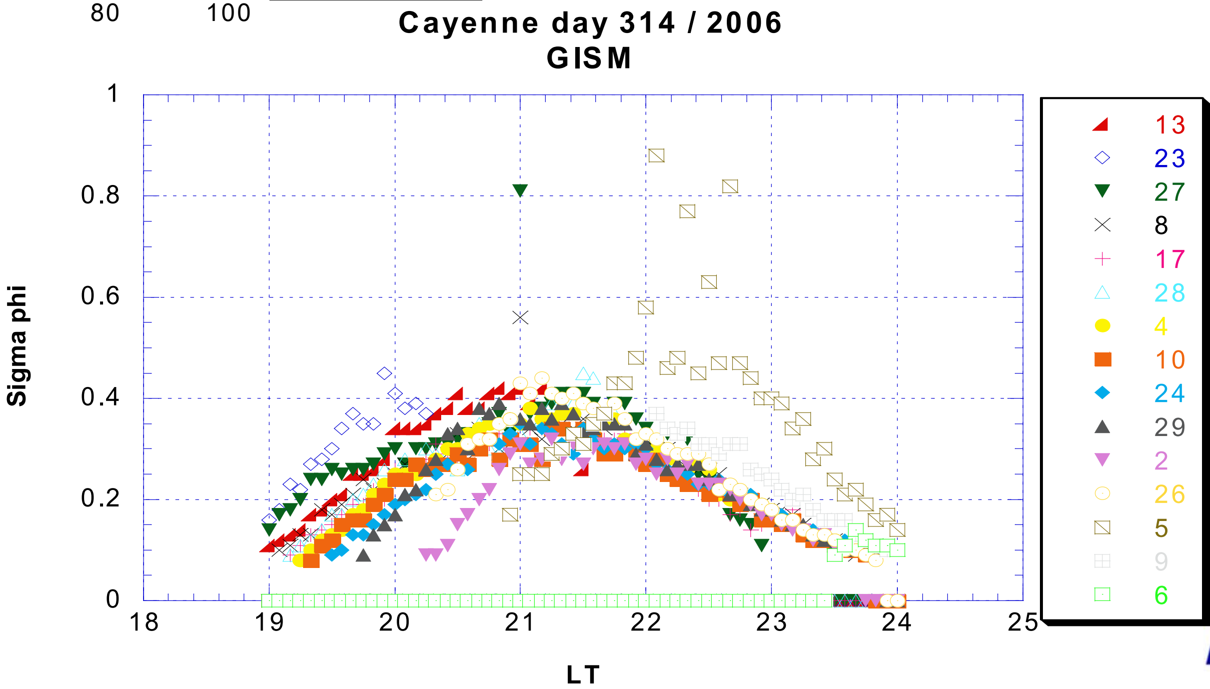

Some samples exhibit high values (both measurements and modelling) due to the cycle slips

Modelling vs Measurements one month of measurements

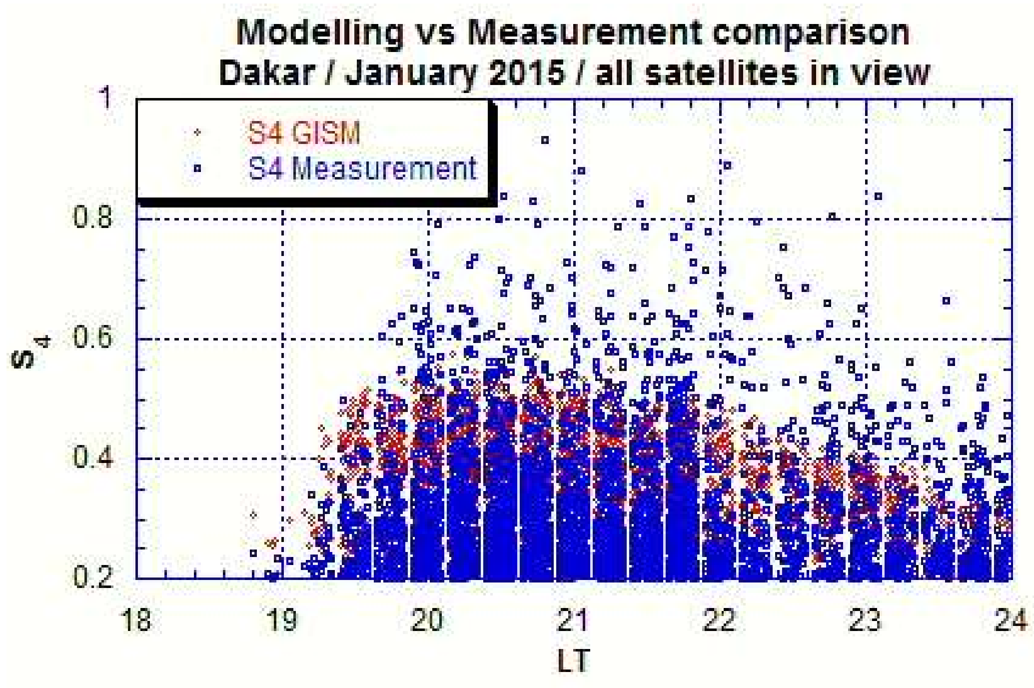

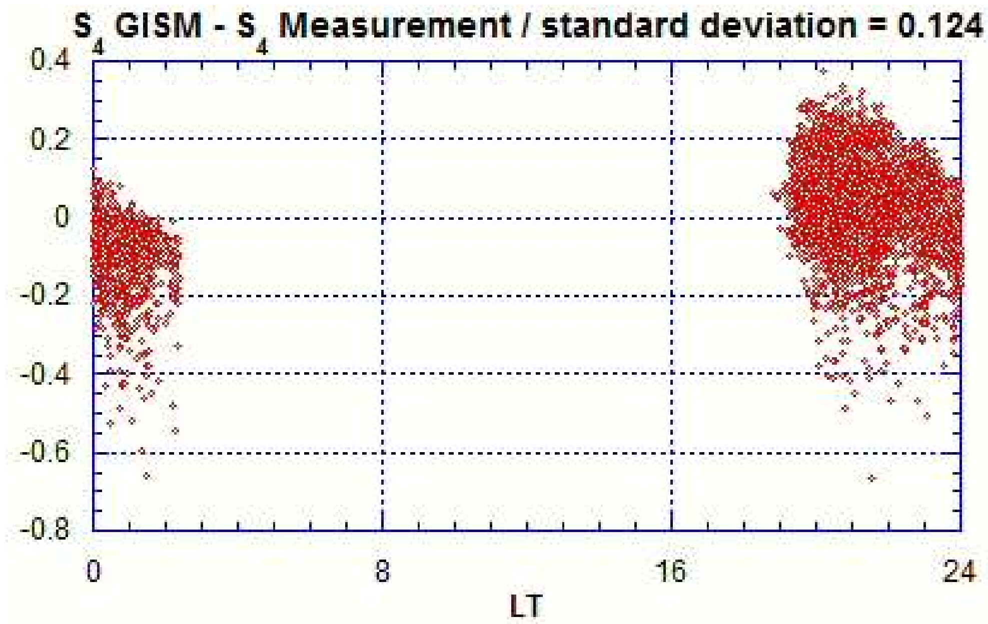

All links considered: input data from the 1 mn pre processed file of recorded data

Positioning Errors

Related to scintillations

Positioning errors from Measurements in Brazil in 2001

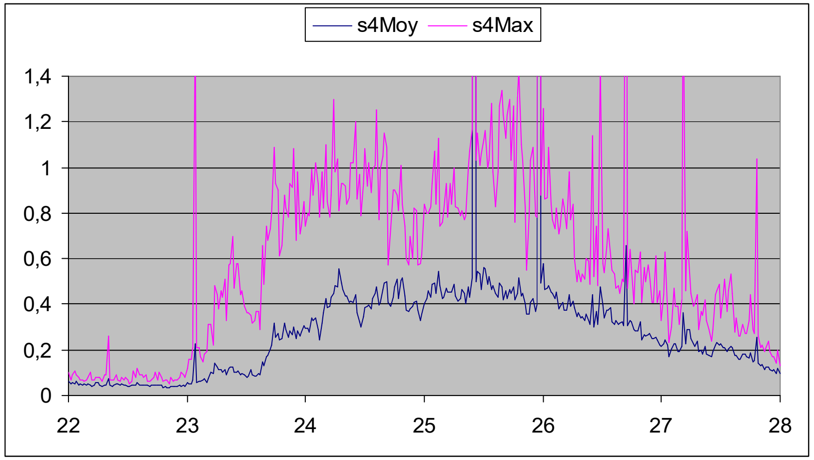

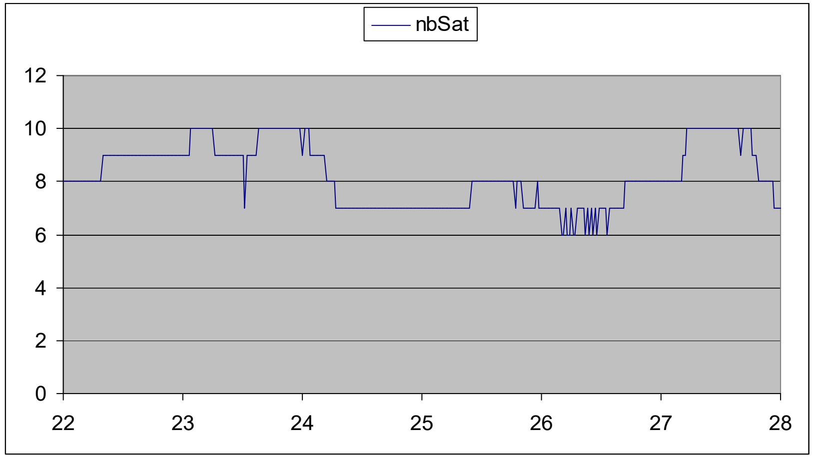

- **Solving the navigation equation**
- **Satellite trajectories obtained from the Yuma files**

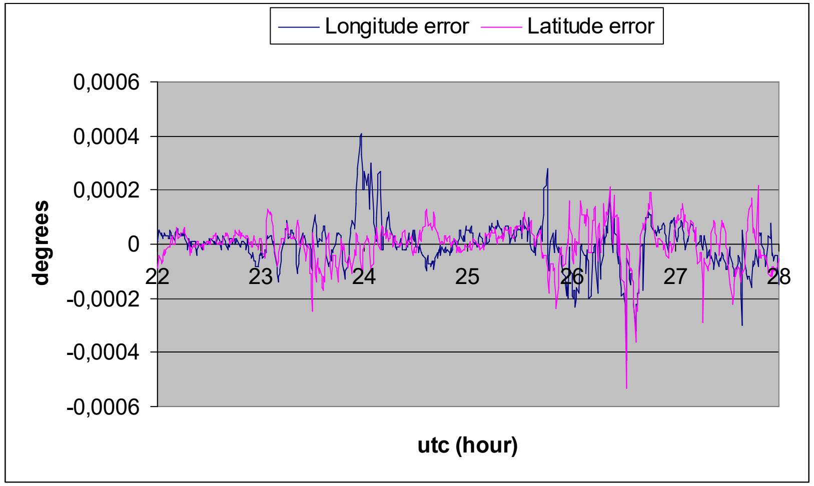

0.0001 degree → 10 meters

Section 4

Extreme events

Storms list

Month with Dst values < -100 nT													
1	2	3	4	5	6	7	8	9	10	11	12	Month	Count
J	F	M	A	M	J	J	A	S	O	N	D	Year	per Year
		x						xx	x			2011	4
		x	x			x			xx	x		2012	6
		x			xx	x						2013	4
	xx		xx									2014	4
		x			x						x	2015	3
xx					x				x			2016	4
				x				x				2017	2
							x					2018	1
2	2	4	3	1	4	2	1	3	4	1	1	Sum: 28	

EGNOS Days of Decrease Performance

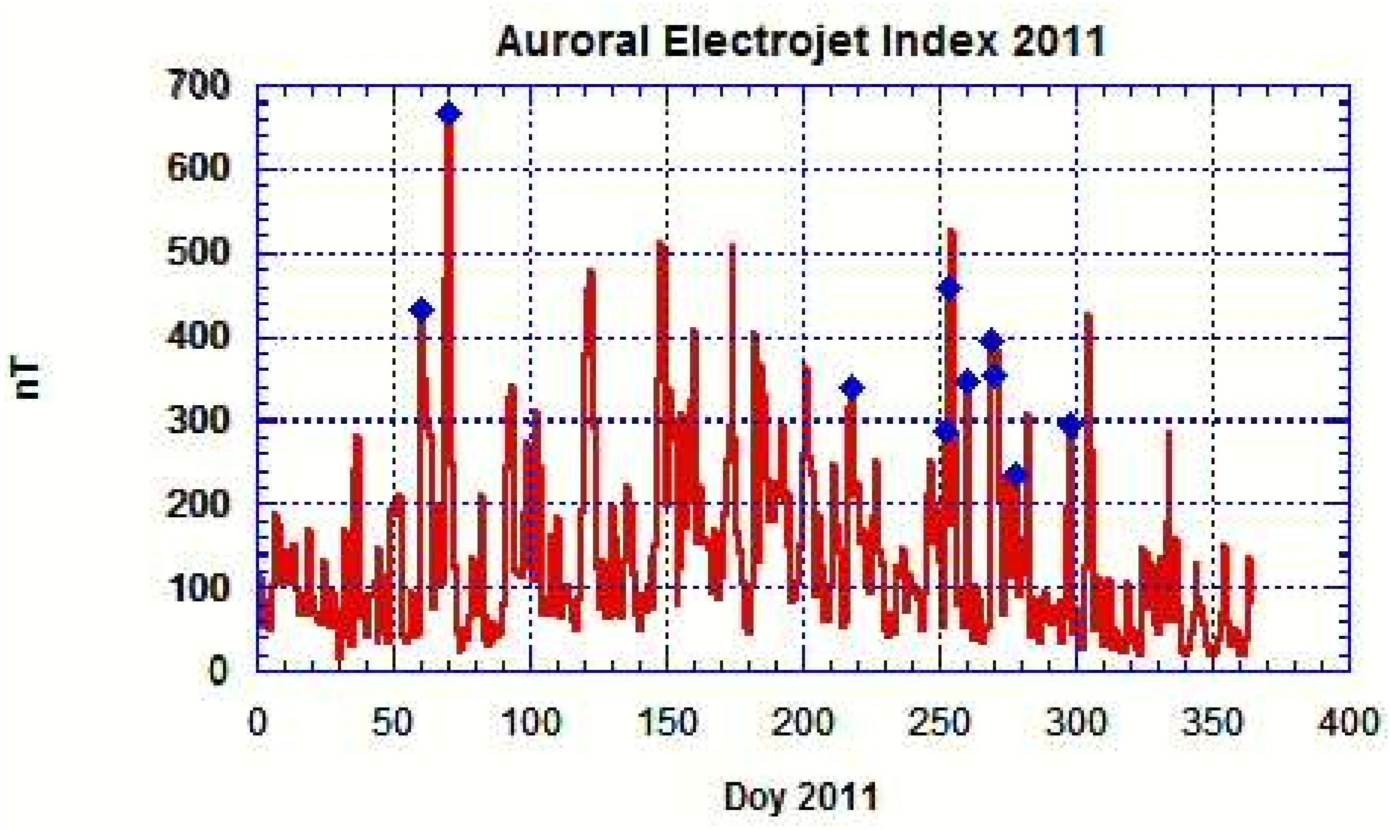

The EGNOS days of decrease of performance were all corresponding to a peak of the magnetic activity

Study Case

St Patrick magnetic storm
17 – 22 march 2015

IEEA

Index detection of the 2015 St Patrick geomagnetic storm

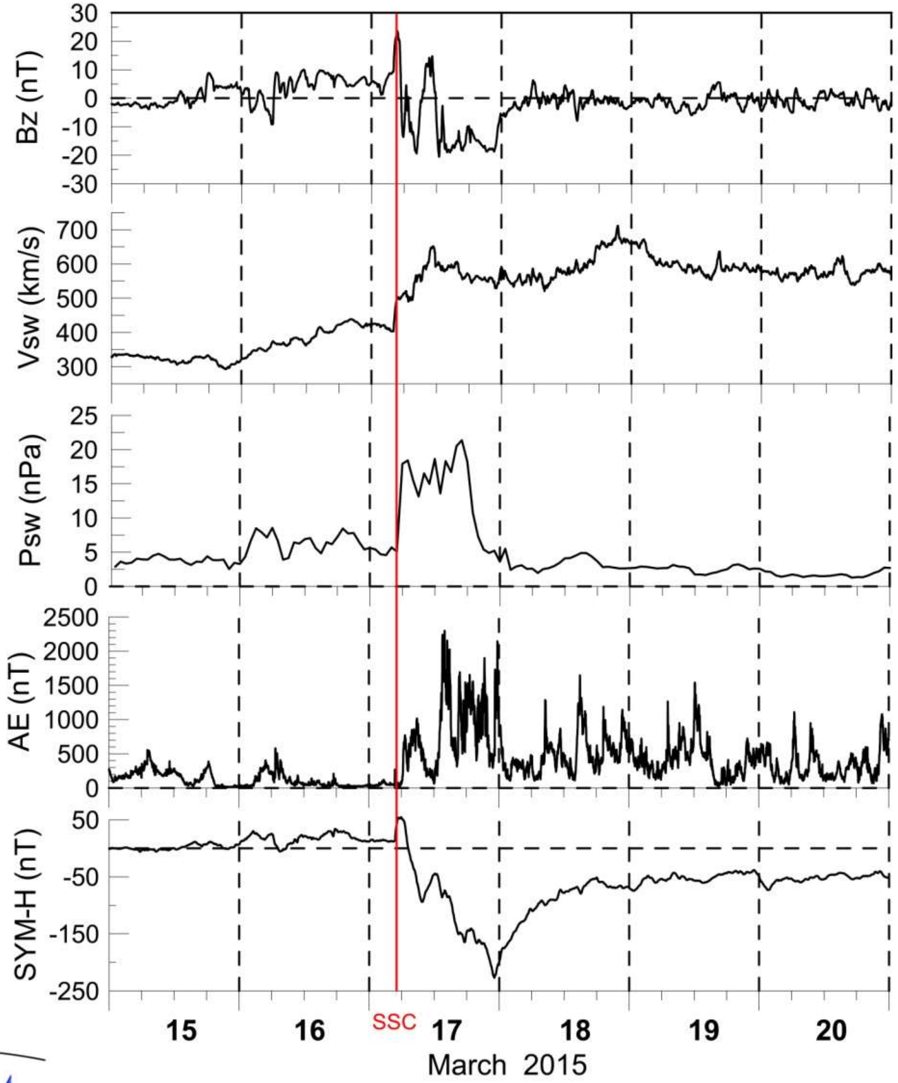

- ➢ Largest storm for the last 10 years
- ➢ Intense particle precipitation
- ➢ Aurora was recorded at mid-latitudes

UNIWERSYTET WARMIŃSKO-MAZURSKI W OLSZTYNIE

IEEA

VTEC snapshots @ 2h from 17/03/2015 (doy 76) 00h to 19/03/2015 (doy 77) 24h

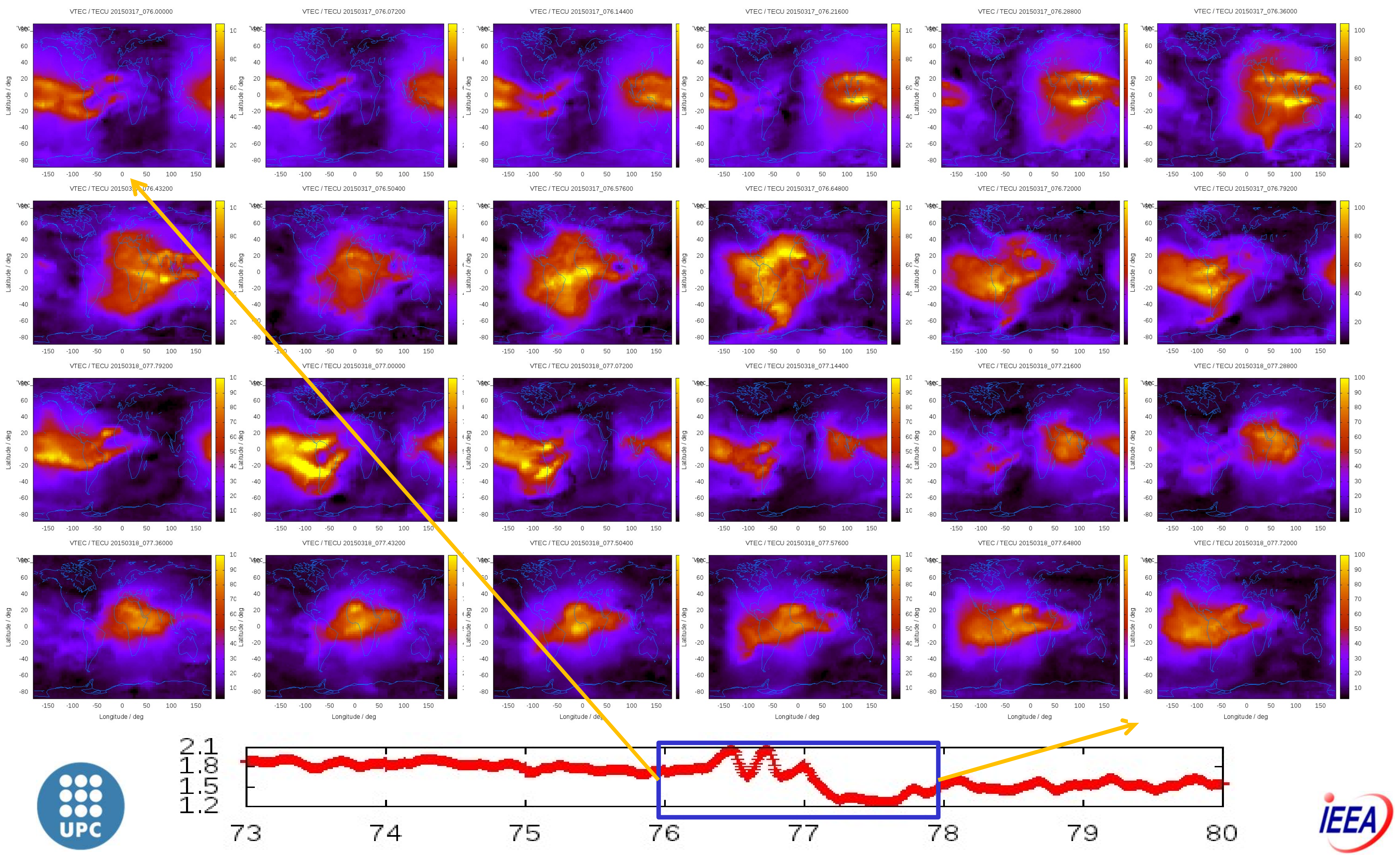

Maps of the Peak Activity

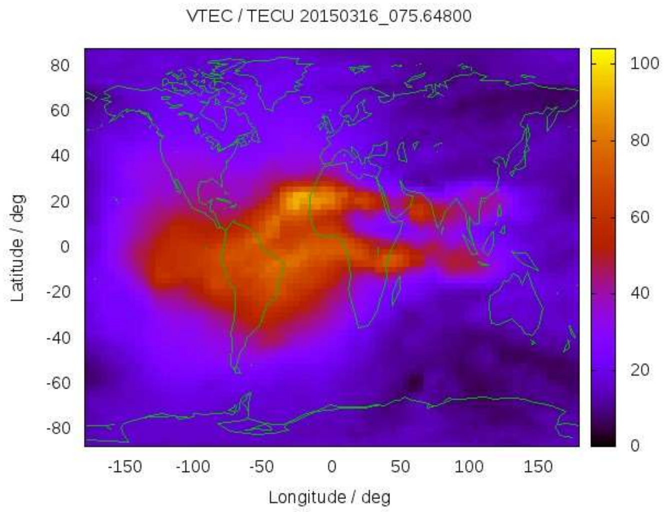

day 75 : 18 h

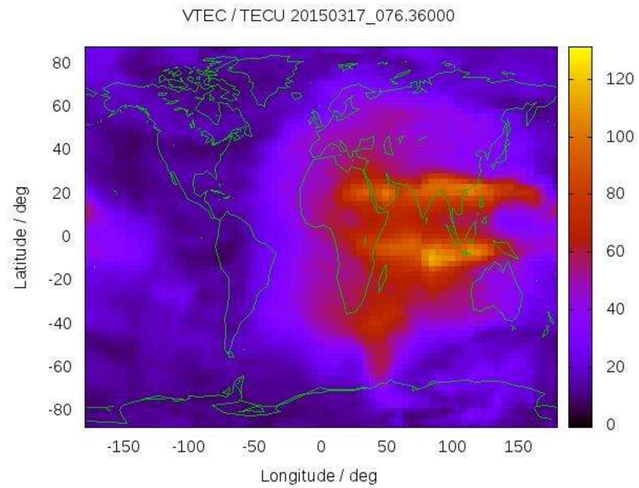

day 76 : 10 h

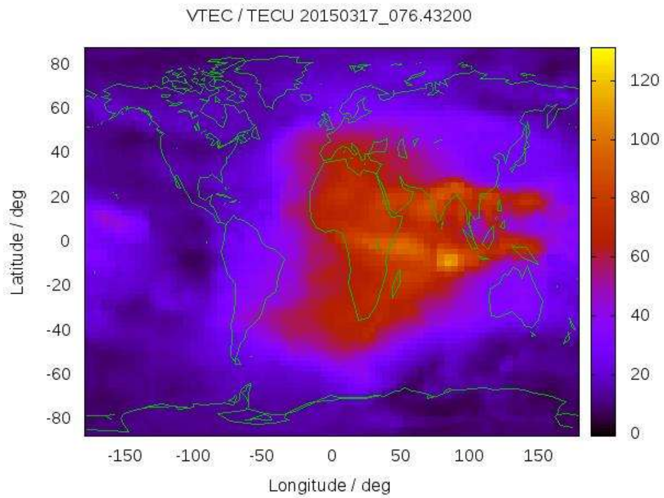

day 76 : 12 h

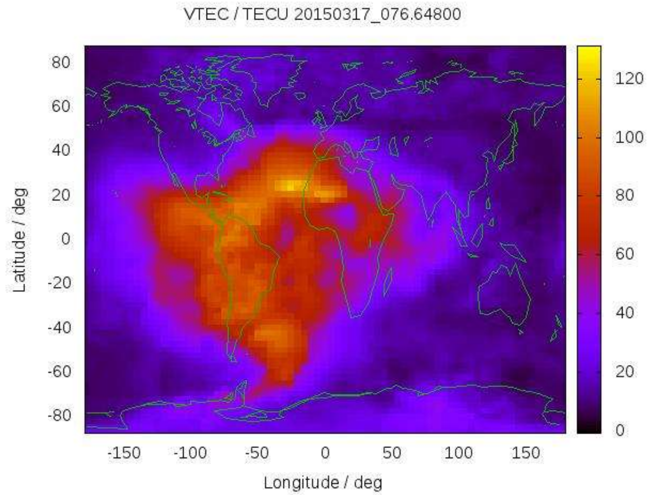

day 76 : 18 h

17/03/2015 (doy 76), to 21/03/2015 (day 80)
Availability maps

(from https://egnos-user-support.essp-sas.eu/new_egnos_ops/?q=apv1_availability)

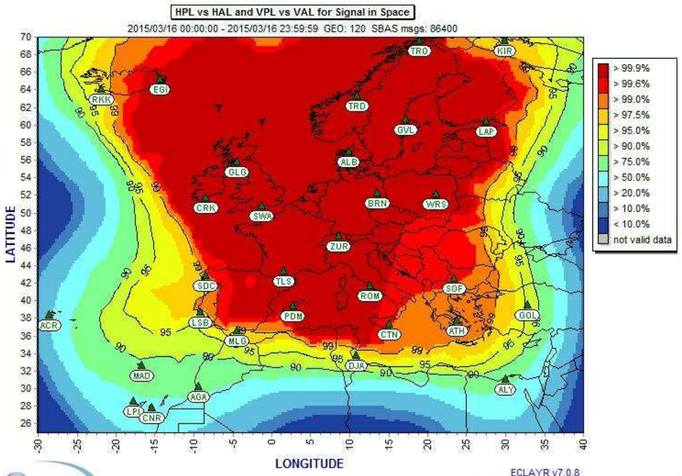

16 march

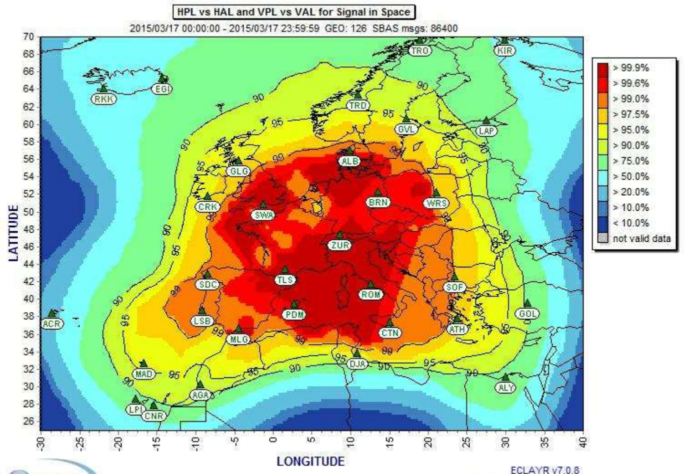

17 march

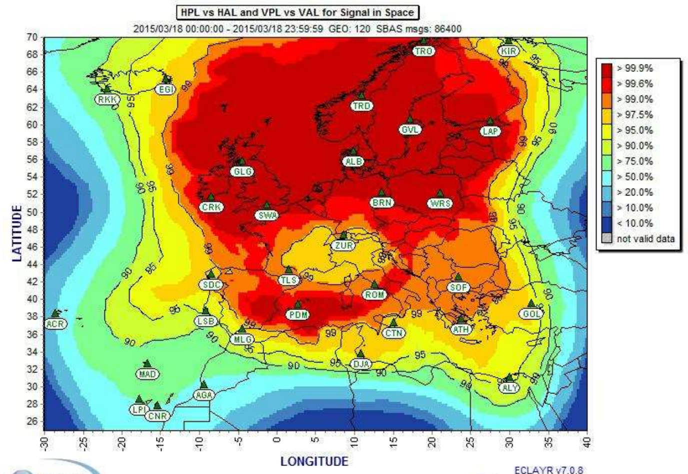

18 march

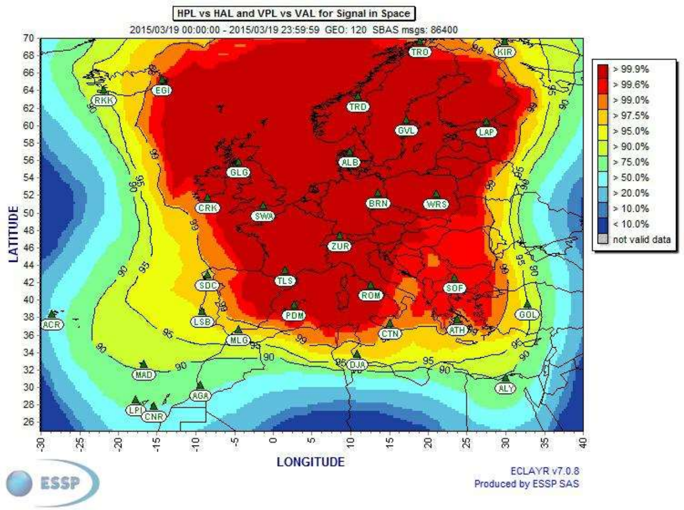

19 march

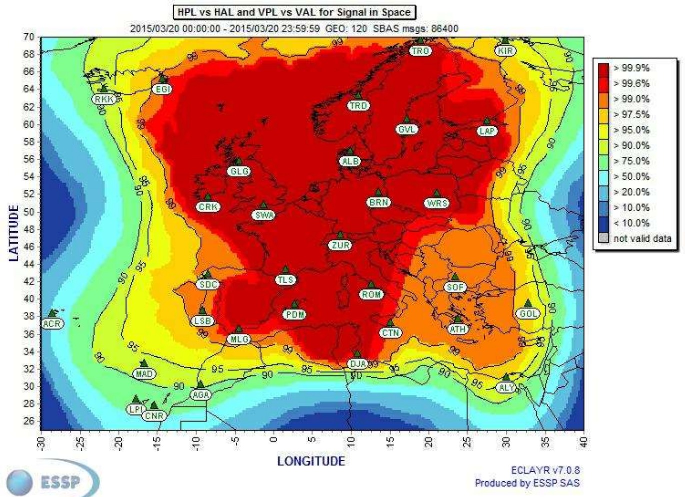

20 march

Conclusion

- **Scintillation occurrence & Probabilities**
  - Low latitudes : The probability of scintillation events was derived depending on the season, latitude and local time for one and several satellites
  - High latitudes : relationship to the magnetic activity
- **Raw data analysis**
  - Fade and inter fades durations & probabilities were given, depending on the S4 value.
  - Signal Correlation characteristics
- **Modelling : GISM (phase screen model)**
- **Extreme events (EGNOS performance loss)**

IEEA

References

- Vasylyev D., Béniguel Y., Wilken V., Kriegel M., Berdermann J., “Modelling of ionospheric scintillation”, *J. Space Weather Space Climate*, 12, 22

- Béniguel Y., I. Cherniak, A. Garcia-Rigo, P. Hamel, M. Hernández-Pajares, R. Kameni, A. Kashcheyev, A. Krankowski, M. Monnerat, B. Nava, Herbert Ngaya, R. Orus - Perez, H. Secrétan, D. Sérant, S. Schlüter, V. Wilken, “MONITOR Ionospheric Network: Two case studies on Scintillation and Electron Content Variability”, Annals of Geophysicae, doi:10.5194/angeo-35-377-2017

- “Effects of ionospheric scintillations on GNSS, A white paper”, SBAS Iono Group : BC, Stanford, Mitre, JPL, NB University, ESA, IEEA, ICTP, …, 2010

- JP Adam, Y. Béniguel, N. Jakowski, T. Noack, V. Wilken, M. Cueto, A. Bourdillon, JJ. Valette, P. Lassudrie – Duchesne, B. Arbesser Rastburg, “Analysis of scintillations recorded during the PRIS measurement campaign”, Ionospheric Effects Symposium, IES 2008, 13 – 15 mai 2008, Alexandria, Va, USA

- Béniguel Y., P. Hamel, “A Global Ionosphere Scintillation Propagation Model for Equatorial Regions”, Journal of Space Weather Space Climate, 1, (2011), doi: 10.1051/swsc/2011004